Article

Neuron

Epigenetic Signaling in Glia Controls Presynaptic Homeostatic Plasticity

Highlights

- Multiple SAGA complex genes are essential for presynaptic homeostasis
- The SAGA complex acts specifically within glia during presynaptic homeostasis
- Glial SAGA regulates the extracellular matrix to stabilize synaptic homeostasis
- Glutamate receptor function is linked to a systemic, glial, epigenetic response

Authors

Tingting Wang, Danielle T. Morency, Nathan Harris, Graeme W. Davis

Correspondence

graeme.davis@ucsf.edu

In Brief

Homeostatic plasticity stabilizes neural function throughout life and, if impaired, renders the nervous system less robust to injury, infection, and disease. Wang and colleagues demonstrate that the homeostatic control of neurotransmitter release requires epigenetic signaling factors that reside in glia. Their study argues for glial-dependent, epigenetic specification of the neuronal extracellular environment that is essential for the induction and maintenance of homeostatic plasticity. The data may have relevance for neurological and psychiatric disorders associated with impaired epigenetic signaling.

Wang et al., 2020, Neuron *105*, 1–15
February 5, 2020
https://doi.org/10.1016/j.neuron.2019.10.041

CellPress

Please cite this article in press as: Wang et al., Epigenetic Signaling in Glia Controls Presynaptic Homeostatic Plasticity, Neuron (2019), https://doi.org/10.1016/j.neuron.2019.10.041

Neuron
Article

Epigenetic Signaling in Glia Controls Presynaptic Homeostatic Plasticity

Tingting Wang,[1,2,3] Danielle T. Morency,[2] Nathan Harris,[1] and Graeme W. Davis[1,4,*]
[1]Department of Biochemistry and Biophysics, Kavli Institute for Fundamental Neuroscience, University of California, San Francisco, San Francisco, CA 94158, USA
[2]Interdisciplinary Program in Neuroscience, Georgetown University Medical Center, Washington, DC 20057, USA
[3]Present address: Department of Pharmacology and Physiology, Georgetown University Medical Center, Washington, DC 20057, USA
[4]Lead Contact
*Correspondence: graeme.davis@ucsf.edu
https://doi.org/10.1016/j.neuron.2019.10.041

SUMMARY

Epigenetic gene regulation shapes neuronal fate in the embryonic nervous system. Post-embryonically, epigenetic signaling within neurons has been associated with impaired learning, autism, ataxia, and schizophrenia. Epigenetic factors are also enriched in glial cells. However, little is known about epigenetic signaling in glia and nothing is known about the intersection of glial epigenetic signaling and presynaptic homeostatic plasticity. During a screen for genes involved in presynaptic homeostatic synaptic plasticity, we identified an essential role for the histone acetyltransferase and deubiquitinase SAGA complex in peripheral glia. We present evidence that the SAGA complex is necessary for homeostatic plasticity, demonstrating involvement of four new genes in homeostatic plasticity. This is also evidence that glia participate in presynaptic homeostatic plasticity, invoking previously unexplored intercellular, homeostatic signaling at a tripartite synapse. We show, mechanistically, SAGA signaling regulates the composition of and signaling from the extracellular matrix during homeostatic plasticity.

INTRODUCTION

The homeostatic modulation of presynaptic neurotransmitter release, termed presynaptic homeostatic potentiation (PHP), is a fundamental form of neural regulation. It is highly conserved from *Drosophila* to human (Davis, 2013; Davis and Müller, 2015). PHP can be initiated by the loss or inhibition of postsynaptic glutamate receptors and is expressed as a compensatory enhancement of presynaptic vesicle release (Frank et al., 2006; Petersen et al., 1997). Large-scale forward genetic screens have identified numerous genes that function within the pre- and postsynaptic elements that are essential for the initiation and expression of presynaptic homeostatic plasticity. Yet, to date, there has been no evidence that glia participate in the mechanisms of PHP, nor has there been any evidence for the participation of epigenetic gene regulation.

Epigenetic regulation of gene expression has a profound impact on neuronal cell-fate specification and neural circuit development in the embryonic nervous system (Baizabal et al., 2018; Yao et al., 2016). The importance of epigenetic control of gene expression is evident based on the numerous neurodevelopmental, neuropsychiatric, and neurodegenerative disorders that have been associated with loss of epigenetic controls including Rett syndrome, fragile X, autism, schizophrenia, spinocerebellar ataxia (SCA), and amyotrophic lateral sclerosis (ALS) (Amir et al., 1999; Coffee et al., 1999; De Rubeis et al., 2014; Jimenez-Pacheco et al., 2017; Lindblad et al., 1996; Sun et al., 2016; Tsankova et al., 2007). It has become clear that epigenetic gene regulation is dynamic and sensitive to changes in neuronal function in both the developing and mature nervous systems. Epigenetic factors that function within neurons have been demonstrated to influence both Hebbian and non-Hebbian neural plasticity (Guzman-Karlsson et al., 2014). Specifically, levels of histone acetylation and DNA methylation within neurons have been associated with, and are required for, normal long-term potentiation (LTP) and memory formation (Gräff and Tsai, 2013; Guzman-Karlsson et al., 2014). Multiple neuronal epigenetic factors have also been linked to non-Hebbian postsynaptic quantal scaling (Benevento et al., 2016; Blackman et al., 2012; Meadows et al., 2015; Yu et al., 2015).

The bulk of existing information underscores the importance of epigenetic signaling within neurons. Less is known about epigenetic gene regulation in glia. This is particularly true with respect to Hebbian and homeostatic plasticity but also applies to neurological and psychiatric disease. This gap in knowledge exists despite the fact that glia are key players that control many aspects of neural development including synaptogenesis, synapse refinement, circuit maturation, and quantal scaling (Beattie et al., 2002; Christopherson et al., 2005; Eroglu et al., 2009; Singh et al., 2016; Stellwagen and Malenka, 2006; Stogsdill et al., 2017) and are increasingly linked to neurodegenerative pathology (Hong et al., 2016; Stevens et al., 2007). The evidence in favor of an essential function for epigenetic signaling in glia exists primarily in the context of nerve injury (Arthur-Farraj et al., 2017; Koreman et al., 2018; Staszewski and Prinz, 2014). As yet, there is no direct evidence demonstrating that epigenetic signaling or glia is necessary for either the induction or expression of PHP.

Here, we demonstrate that multiple genes encoding members of the Spt-Ada-Gcn5 acetyltransferase and deubiquitinase (SAGA) complex are specifically required in peripheral glia for presynaptic homeostatic plasticity. The SAGA complex is a prominent histone acetyltransferase protein complex that is conserved from yeast to human (Helmlinger and Tora, 2017; Lee and Workman, 2007). Remarkably, SAGA-dependent signaling is not constrained to the synapse but appears to propagate throughout the extracellular space surrounding the synapse, axon, soma, and dendrites. This represents a shift in the composition of the extracellular environment of the entire neuron during homeostatic plasticity. We propose that glial-dependent, epigenetic specification of the extracellular neuronal environment may be a general mechanism that is necessary for the life-long maintenance of homeostatic plasticity, existing for months in *Drosophila* (Mahoney et al., 2014), years in mice (Plomp et al., 1992), and decades in human (Cull-Candy et al., 1980).

RESULTS

The SAGA Complex Components Ada2b and Sgf11 Are Necessary for PHP

The SAGA complex in *Drosophila* is composed of approximately 20 proteins, encompassing histone acetyltransferase and deubiquitinase catalytic activities (Weake and Workman, 2012). An ongoing effort to screen for genes involved in homeostatic plasticity identified a potential function for *ada2b* during PHP, and this was subsequently expanded to a test of four genes, all components of the SAGA complex: two acetyltransferases *ada2b* (*ada2b*^{1}; Qi et al., 2004) and *gcn5* (*gcn5*^{E333st}/*gcn5*^{Q186st}; Carré et al., 2005) and two deubiquitinases *sgf11* (*sgf11*^{e01308}; Weake et al., 2008) and *non-stop* (Weake et al., 2008; Figure 1A). First, we demonstrated that loss of these individual genes impairs the rapid induction of synaptic homeostasis. Bath application of 15 μM Philanthotoxin (PhTX) induced an ~50% reduction of the average miniature excitatory postsynaptic potential amplitude (mEPSP amplitude) at the neuromuscular junction (NMJ; Figures 1B–1D). In the wild type, an increase in presynaptic release (quantal content; Figures 1C and 1F) was observed that offset the change in mEPSP amplitude and restored postsynaptic excitation to baseline values (Figure 1E). By contrast, there is no change in quantal content in the *ada2b*, *gcn5*, or *sgf11* mutants (Figures 1C and 1F). As a consequence, average excitatory postsynaptic potential (EPSP) amplitude at mutant synapses is significantly smaller in the presence of PhTX compared to the absence of PhTX (Figure 1E). Thus, three independent genes, all members of the SAGA complex, encompassing two different enzymatic activities, are essential for the rapid induction of PHP.

Next, we assessed whether the SAGA complex is required for the long-term maintenance of PHP, induced by genetic deletion of the postsynaptic glutamate receptor subunit GluRIIA (Petersen et al., 1997; Figures 1G and 1I). We examined two different *GluRIIA* and SAGA double-mutant combinations: *GluRIIA;ada2b*^{1} and *GluRIIA;sgf11*^{e01308}. In both double mutants, the mEPSP amplitudes are significantly decreased (Figures 1G and 1H), and the homeostatic regulation of presynaptic release is completely blocked (Figures 1G and 1J). As a consequence, EPSP amplitudes are significantly decreased in the double mutants compared to the same genotype alone at baseline. Based on these data, we propose that the SAGA complex is necessary for both the rapid induction and maintenance of presynaptic homeostasis.

Ada2b Is Necessary in Peripheral Glia for PHP

In order to examine the specific cell type in which the *Drosophila* SAGA complex functions during presynaptic homeostasis, we tested SAGA activity in motoneurons, muscle, and in peripheral glia using tissue-specific, RNAi-mediated, gene knockdown (Figure 2). Specifically, we expressed *UAS-ada2b RNAi* in motoneurons (*OK371-Gal4*), muscle (*MHC-Gal4*), perineurial glia (*Egr-Gal4*, Keller et al., 2011; *NP6293-Gal4*, Awasaki et al., 2008; Stork et al., 2012), and astrocyte-like glia (*Alrm-Gal4*, Doherty et al., 2009; Stork et al., 2012). We demonstrated that PhTX-induced synaptic homeostasis was completely normal when *ada2b-RNAi* was expressed in either mononeurons or muscle (Figures 2C and S1). However, when *ada2b-RNAi* was expressed in perineurial glia, we found a complete block of PHP (Figures 2C, 2D, and S1). We also demonstrated that perineurial glia, identified by expression of *Egr-Gal4* and *NP6293-Gal4*, extended to the NMJ (Figure 2B). Although these glia do not extend along the full length of the presynaptic nerve terminal, they are localized in close proximity to presynaptic boutons at the NMJ (Figure 2B). This is consistent with prior ultrastructural data examining glial morphology at the site of nerve-muscle contact in third-instar larvae and other prior reports (Brink et al., 2012; Keller et al., 2011; Kerr et al., 2014).

We have performed a series of control experiments to confirm a role for *ada2b* within perineurial glia during post-embryonic development. First, we confirmed the identity and specificity of the perineurial glial *Gal4* drivers (Figure S2). We also characterized the identity of *Egr* positive cells in the peripheral glia. The percentage of total peripheral glia that are labeled by *Egr-Gal4* is similar to *NP6293-Gal4*, a confirmed perineurial *Gal4* driver (Awasaki et al., 2008; Stork et al., 2012; Figures S2B and S2C). Moreover, when we used both *Gal4* drivers to express *UAS-GFP* with a nucleus localization sequence (*UAS-GFP.nls*), the ratio of GFP positive nuclei to all glial nuclei is unchanged, indicating that *Egr-Gal4* and *NP6293-Gal4* label largely overlapping, if not the same population of peripheral glia (Figure S2B). Both *Egr-Gal4* and *NP6293-Gal4* block PHP when used to express *UAS-ada2b RNAi*, arguing for peripheral glial-specific activity that is likely localized to perineurial glial cells, as defined by these *Gal4* lines.

Next, we addressed the possibility that *ada2b* functions during early embryonic development to affect synapse function. To address this issue, we used a temperature-sensitive *Tubulin-Gal80*^{ts} driver, combined with *NP6293-Gal4*, to induce the expression of *UAS-ada2b RNAi* only during post-embryonic larval development. We demonstrate that presynaptic homeostatic plasticity is still impaired at the NMJ when *ada2b* is disrupted in perineurial glia following the completion of embryonic development (Figure 2E; temperature shift 18°C–29°C initiated 30 h after egg laying).

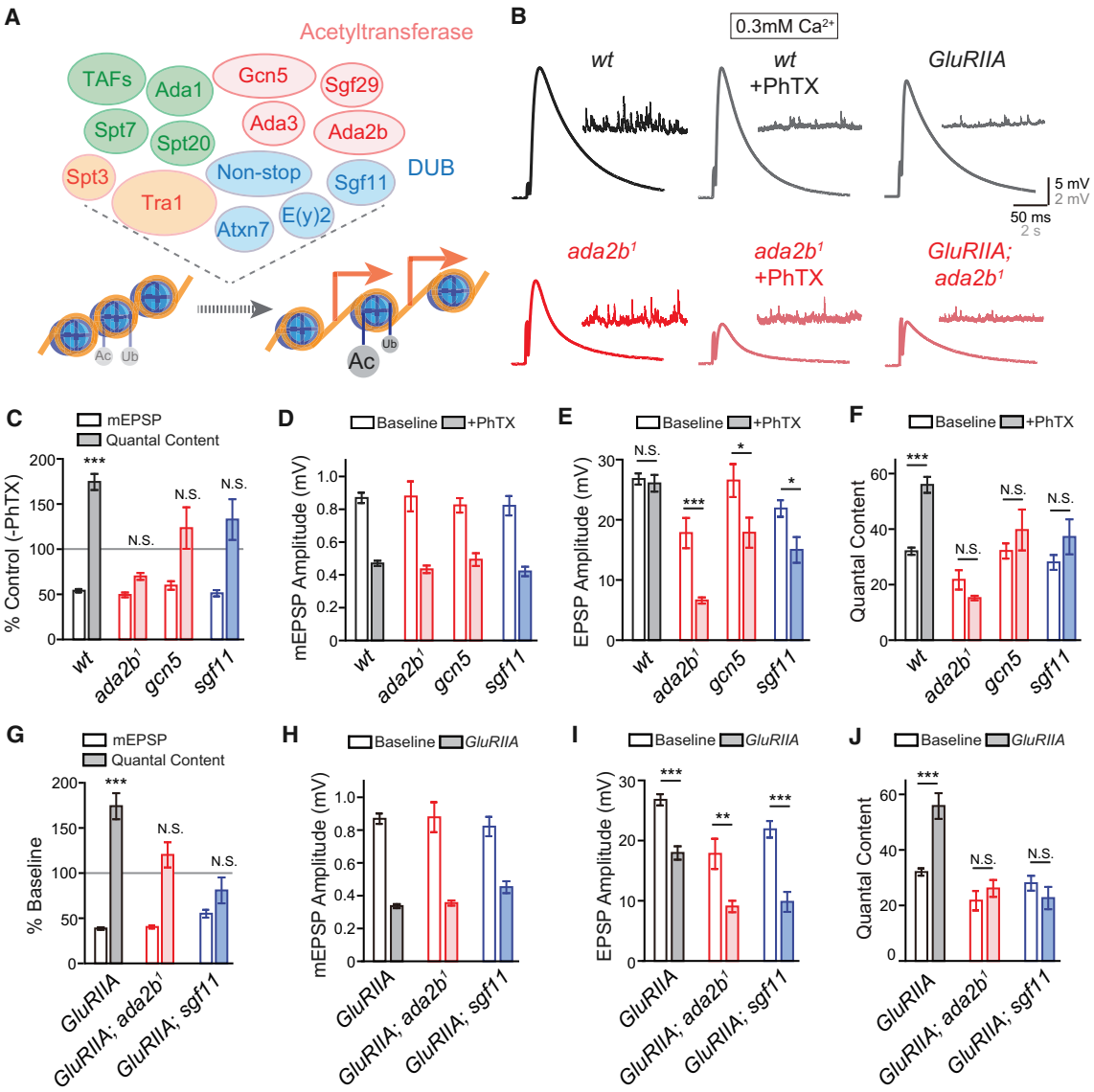

Figure 1. SAGA Complex Gene Mutations Block PHP

(A) Diagram of the Acetyltransferase (red) and Deubiquitinase (DUB, blue) modules in the SAGA complex in *Drosophila* (top panel). Other components include structural (green) and transcription factor (TF) binding and transcription factor binding protein (TBP) binding modules (orange). Acetylation and deubiquitination of histone H3 lead to relaxed chromatin structure and active gene transcription (red arrows, bottom panel).

(B) Representative EPSP and mEPSP traces in wild type (WT, black) and the *ada2b*^{1} mutant (*ada2b*^{1}, red) in the absence (–PhTX) and the presence of philanthotoxin (+PhTX). At far right, the *GluRIIA* mutant and *GluRIIA;ada2b*^{1} double mutant are shown.

(C) mEPSP amplitudes (open bars) and presynaptic release (quantal content, filled bars). Data for each genotype are presented as the percentage of change in PhTX compared to the same genotype recorded in the absence of PhTX. Genotypes: WT, *ada2b* (*ada2b*^{1}), *gcn5* (*gcn5*^{E333st}/*gcn5*^{Q186st}), *sgf11* (*sgf11*^{e01308}). Mean ± SEM; ***p < 0.001, N.S., not significant; Student's t test for pairwise comparisons within a genotype ± PhTX.

(D–F) Non-normalized values for analysis of the mutants in (C). Average mEPSP amplitude (D), EPSP amplitude (E), and presynaptic release (quantal content; F) in the absence (open) and presence (filled bars) of PhTX. Genotypes as in (C). Mean ± SEM; *p < 0.05, ***p < 0.001, N.S.; Student's t test for pairwise comparisons within a genotype ± PhTX.

(G) mEPSP amplitudes (open bars) and presynaptic release (quantal content, filled bars). Data for each genotype are presented as the percentage of change in PhTX compared to the same genotype recorded in the absence of PhTX.. (H)-(J) Non-normalized values for analysis of the mutants in (G). Average mEPSP amplitude (H), EPSP amplitude (I), and presynaptic release (quantal content; J) in the absence (open) and presence (filled bars) of PhTX. Genotypes as in (G). The following genotypes are presented: *GluRIIA* (gray bars), *GluRIIA;ada2b*^{1} double mutants (red bars), *GluRIIA;sgf11*^{e01308} mutants (blue bars). Mean ± SEM; *p<0.05, **p < 0.01, ***p < 0.001, N.S; Student's t test for pairwise comparisons.

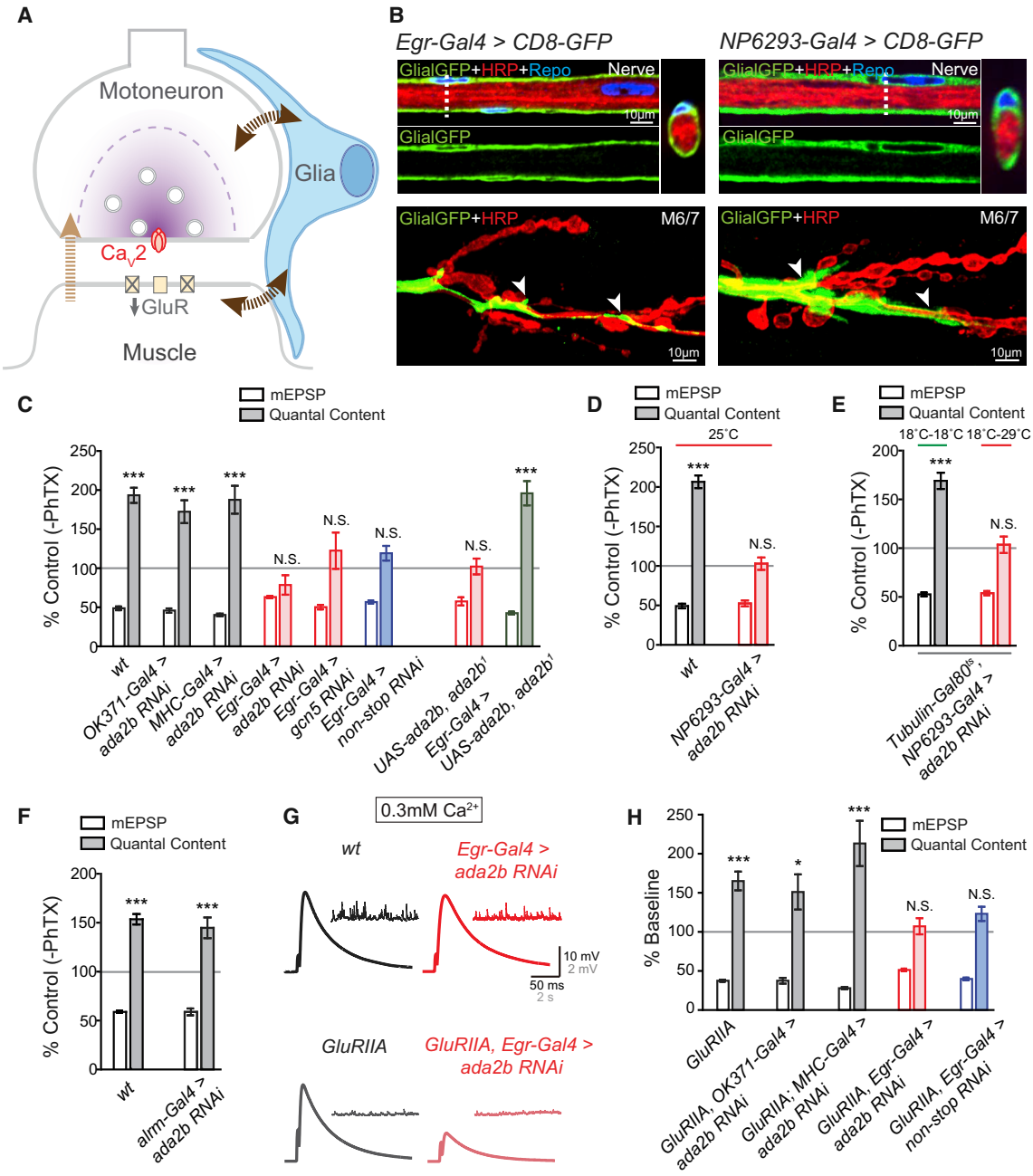

Figure 2. Loss of SAGA Complex Gene Expression within Glia Impairs PHP

(A) Schematic of the *Drosophila* NMJ. Inhibition of postsynaptic glutamate receptor sensitivity leads to a calcium-channel dependent increase of presynaptic release in motoneurons. Glia (blue) are present at the NMJ. In addition to a retrograde signal from muscle to motoneurons (light brown arrow), signaling to and from glia (dark brown arrows) could also contribute to presynaptic homeostatic plasticity.

(B) Representative confocal sections of peripheral glia surrounding the axon bundle in the peripheral nerve. Glial-specific expression of *UAS-CD8-GFP* (*Egr-Gal4 > CD8-GFP*, Glial-GFP, green, left panel; *NP6293-Gal4>CD8GFP*, Glial-GFP, green, right panel), neuronal membrane (anti-horseradish peroxidase [HRP], red), and glial nuclei (immunolabeling for Repo, blue). Dotted vertical line indicated site of optical cross-section, shown at the top panel on the right, rotated 90°. Bottom, the distribution of glia membrane at the NMJ of muscles 6 and 7 (M6/7). White arrows indicate the localization of glia at the NMJ.

(C) mEPSP amplitudes (open bars) and presynaptic release (quantal content, filled bars). Data for each genotype are presented as the percentage of change in PhTX compared to the same genotype recorded in the absence of PhTX. Genotypes were as follows: WT (gray bars), motoneuron-specific knockdown of *ada2b* (*OK371-Gal4 > ada2b RNAi*, gray bars), muscle-specific knockdown of *ada2b* (*MHC-Gal4 > ada2b RNAi*, gray bars), glial-specific knockdown of *ada2b* (*Egr-Gal4 > ada2b RNAi*, red bars), glial-specific knockdown of *gcn5* (*Egr-Gal4 > gcn5 RNAi*, red bars), glial-specific knockdown of *non-stop* (*Egr-Gal4 > non-stop RNAi*, blue bars), heterozygous *UAS-ada2b* in the homozygous *ada2b*^{1} mutant background without a *Gal4* driver (*UAS-ada2b,ada2b*^{1}), and glial-specific expression of *UAS-ada2b* in *ada2b*^{1}mutant (*Egr-Gal4 > UAS-ada2b,ada2b*^{1}). Mean ± SEM; ***p < 0.001, N.S.; Student's t test.

(legend continued on next page)

Next, we performed tissue-specific genetic rescue experiments. We expressed *UAS-ada2b* specifically in glia in the *ada2b*^{1} mutant and fully restored PHP in the *ada2b*^{1} mutant background (Figure 2C). Note that PhTX-induced synaptic homeostasis remained completely blocked in *ada2b*^{1} mutants harboring only the *UAS-ada2b* transgene without a source of *Gal4* present (Figure 2C), emphasizing that the rescue of PHP is due to *Gal4*-mediated overexpression of *UAS-ada2b* in glia.

Finally, we asked whether the SAGA complex also functions in other glial cell types within the CNS during PHP. In particular, astrocyte-like glial cells populate the *Drosophila* CNS (Stork et al., 2012) and astrocytes are known to participate in other forms of homeostatic plasticity in mammalian cultured neurons (Stellwagen and Malenka, 2006). We used the previously characterized astrocyte-like glial *Gal4* driver *Alrm-Gal4* (Doherty et al., 2009; Stork et al., 2012) to drive the expression of *UAS-ada2b RNAi* and observed normal homeostatic plasticity. These data suggest that *ada2b* is not necessary in astrocyte-like glia, within the CNS for synaptic homeostasis at the NMJ (Figure 2F).

Additional SAGA Components, Non-Stop and Gcn5, Are Necessary for PHP

We have extended our analysis of the SAGA complex to include two additional genes: *non-stop* and *gcn5*. The *non-stop* gene encodes a deubiquitinase enzyme and *gcn5* has acetyltransferase activity (Figure 1). When we used *Egr-Gal4* to drive the expression of either *UAS-gcn5 RNAi* or *UAS-non-stop RNAi*, we found that the rapid induction of homeostatic plasticity was blocked (Figure 2C). These data are consistent with a general requirement for the activity of SAGA complex for the normal expression of PHP.

Finally, we tested the sustained expression of PHP. When either *UAS-ada2b RNAi* was driven in motoneurons or muscles in the *GluRIIA* mutant background, we observed normal PHP (Figure 2H). However, when *UAS-ada2b RNAi* was driven in glia (*GluRIIA*, *Egr-Gal4 > ada2b RNAi*), the sustained expression of homeostasis was blocked (Figures 2G and 2H). We observed similar impairment of sustained homeostasis when *non-stop* was disrupted specifically in glia in the *GluRIIA* mutant background (Figure 2H). Two conclusions can be made at this point. First, our data demonstrate the essential participation of peripheral glia in both the rapid induction and sustained expression of PHP. Second, we demonstrate that multiple components of the SAGA complex are essential for presynaptic homeostatic plasticity, acting within peripheral glia.

Normal Glial and Synapse Morphology

We examined the morphology of the NMJ and surrounding glia. Loss of *ada2b* expression in glia (*Egr-Gal4 > ada2b RNAi*) had no effect on the shape or distribution of glia within the peripheral nerve or at the NMJ of muscles 6/7 (Figures 3A–3C). Total active zone number, estimated by quantification of Brp puncta number (Marie et al., 2004) is either unaltered following loss of *ada2b* expression in glia (*Egr-Gal4 > ada2b RNAi*; abdominal segment 3), or slightly increased (abdominal segment 2) compared to wild type (Figure 3D). There is a small increase of the total postsynaptic area (region of Dlg immunostaining) at the NMJ following expression of *ada2b RNAi* in glia, but only in abdominal segment 3 (Figure 3E). Finally, there is a slight increase of total bouton number in segment 2 but no change of Brp density in the *ada2b RNAi* mutant (Figures 3F and 3G). In conclusion, although small differences in NMJ anatomy are observed, there are no consistent changes that could account for the block of PHP following glial-specific depletion of *ada2b* expression. Finally, we performed a further control to ensure that *Egr-Gal4* line does not itself interfere with PHP. Eiger (Egr) is the *Drosophila* homolog of mammalian TNF-α, important for homeostatic scaling in mice (Stellwagen and Malenka, 2006). We examined PhTX-induced presynaptic homeostasis in an *egr*-null mutation (*egr*$^{\Delta 25}$; Keller et al., 2011) and demonstrated that PHP was completely normal (Figure S3). This experiment also effectively rules out Eiger as a potential candidate for glial-neuronal signaling downstream of the SAGA complex in peripheral glia for PHP.

Modulation of SAGA-Dependent H3K9 and H3K14 Acetylation during PHP

The next question we address is whether SAGA complex activity is altered, in peripheral glia, following muscle-specific disruption of postsynaptic glutamate receptors. Lysines at position 9 and 14 in histone H3 (H3K9 and H3K14) are direct targets of SAGA complex-dependent acetylation (Carré et al., 2005; Qi et al., 2004; Weake et al., 2008). We acquired antibodies specific for acetylation of H3K9 (H3K9Ac) and H3K14 (H3K14Ac) and assessed the abundance of these epigenetic markers in peripheral glia (Figure S4). The nuclei of peripheral glia are distributed

(D) mEPSP amplitudes (open bars) and presynaptic release (quantal content, filled bars). Data for each genotype are presented as the percentage of change in PhTX compared to the same genotype recorded in the absence of PhTX. Genotypes were as follows: WT (gray bars), perineurial glial-specific knockdown of *ada2b* (*NP6293-Gal4 > ada2b RNAi*, red bars). All animals are raised at 25°C. Mean ± SEM; ***p < 0.001, N.S.; Student's t test. See also Figures S1 and S2.

(E) mEPSP amplitudes (open bars) and presynaptic release (quantal content, filled bars). Data are presented as the percentage of change in PhTX compared to the same genotype recorded in the absence of PhTX. Perineurial glial-specific knockdown of *ada2b* (*Tubulin-Gal80*^{ts}, *NP6293-Gal4 > ada2b RNAi*) at permissive (18°C–29°C, red line) and non-permissive temperatures (18°C–18°C, green line). Mean ± SEM; ***p < 0.001, N.S.; Student's t test.

(F) mEPSP amplitudes (open bars) and presynaptic release (quantal content, filled bars) in astrocyte-specific knockdown of *ada2b* (*Alrm-Gal4 > ada2b RNAi*). Data are presented as the percentage of change in PhTX compared to the same genotype recorded in the absence of PhTX. Mean ± SEM; ***p < 0.001, N.S.; Student's t test.

(G) Representative traces for EPSP and spontaneous mEPSP for WT (black), *GluRIIA* mutant (*GluRIIA*, gray), glial-specific knockdown of *ada2b* (*Egr-Gal4 > ada2b RNAi*, red), and glial-specific knockdown of *ada2b* in the *GluRIIA* mutant background (*GluRIIA,Egr-Gal4 > ada2b RNAi*, light red).

(H) Quantification as in (C). Data for each genotype are expressed as percentage of change compared to the same genotype recorded in the absence of the *GluRIIA* mutation. The following genotypes are presented: *GluRIIA* (gray bars), *GluRIIA,OK371-Gal4 > ada2b RNAi* (gray bars), *GluRIIA;MHC-Gal4 > ada2b RNAi* (gray bars), *GluRIIA,Egr-Gal4 > ada2b RNAi* (red bars), and *GluRIIA,Egr-Gal4 > non-stop RNAi* (blue bars).

Mean ± SEM; *p < 0.05, ***p < 0.001, N.S., not significant; Student's t test.

See also Figures S1 and S2.

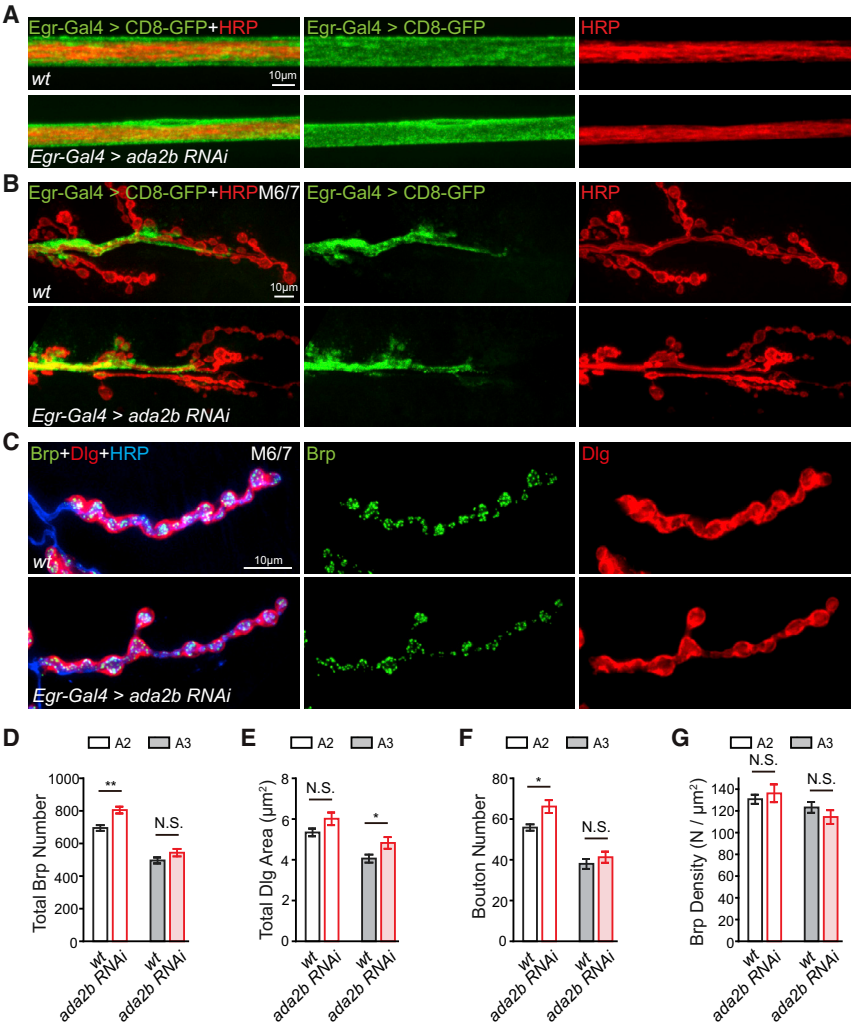

Figure 3. Glial-Specific Impairment of *ada2b* Does Not Affect Glia or Synapse Morphology

(A) Representative confocal images of peripheral glia surrounding a peripheral nerve. Glia, *UAS-CD8-GFP* (green) and neuronal membrane, HRP (red). Glial-specific knockdown of *ada2b* (*Egr-Gal4 > ada2b RNAi*) compared to WT is shown.

(B) Representative confocal images of peripheral glia at the NMJ in WT and *ada2b* mutants (*Egr-Gal4 > ada2b RNAi*), labeling as in (A).

(C) NMJ as in (B) immunolabeled with anti-Bruchpilot (Brp; green, presynaptic), anti-discs large (Dlg; red, postsynaptic), and the neuronal membrane (anti-HRP, blue).

(D–G) The total number presynaptic Brp puncta (D), total area of Dlg (E), total number of synaptic boutons (F), and Brp density (Brp number/Dlg area; G) at muscle 6/7 in abdominal segment 2 (A2, open bars) and segment 3 (A3, filled bars). Genotypes and sample size: *Egr-Gal4 > ada2b RNAi*, n = 7 NMJ for A2, n = 7 NMJ for A3, N = 4 animals, red bars); WT (n = 7 NMJ for A2, n = 7 NMJ for A3, N = 4 animals, black bars).

Mean ± SEM; *p < 0.05, **p < 0.01, N.S. not significant; Student's t test.

See also Figure S3.

throughout the peripheral nerves that extend from the CNS to the musculature. Both anti-H3K9Ac and anti-H3K14Ac immunostaining label the nuclei of peripheral glia (Figure S4). If this labeling is due to SAGA complex activity, then it should be diminished in the *ada2b* mutant. We demonstrated that H3K9Ac and H3K14Ac staining intensity is significantly reduced in the *ada2b*^{1} mutant background compared to wild type (Figures 4A–4F). Finally, we demonstrated that *ada2b*-dependent H3K9Ac and H3K14Ac staining occurs in *Egr-Gal4* positive peripheral glia, the same peripheral glia that are necessary for PHP. Thus, *ada2b* is essential for H3K9Ac and H3K14Ac acetylation in *Egr* positive perineurial glia.

Next, we asked whether H3K9Ac and H3K14Ac staining is altered in the background of the *GluRIIA* mutant. It is important to emphasize that the GluRIIA subunit of the AMPA/Kainate glutamate receptor is only expressed in muscle (Petersen et al., 1997). We demonstrated that both H3K9Ac and H3K14Ac staining intensity in peripheral glia was significantly increased in the *GluRIIA* mutant compared to wild type (Figures 4A–4F). This argues for previously unexplored, PHP-associated signaling from muscle to peripheral glia, inducing a change in histone acetylation. In order to associate the change in glial histone acetylation to the mechanisms of PHP, we demonstrated that enhanced H3K9Ac and H3K14Ac staining intensity was abolished in the *GluRIIA;ada2b*^{1} double mutant, co-incident with the *ada2b*-dependent block of PHP. Since a muscle-specific perturbation (*GluRIIA* deletion mutation) induces an Ada2b-dependent, glial-specific epigenetic change, our data argue for the existence of a signaling system that, directly or indirectly, connects muscle to peripheral glia during PHP. We acknowledge the possibility that other epigenetic codes, such as histone methylation and DNA methylation patterns may also be altered in the *GluRIIA* mutant background.

Independent Evidence that Peripheral Glia Participate in PHP

To provide further evidence of a required function of peripheral glia during PHP, we sought other ways to impair glial function, independent of the SAGA complex mutations. The Sar1-GTPase is necessary for secretory trafficking from the endoplasmic reticulum (ER) to the Golgi apparatus (Ye et al., 2007). Depleting Sar1 should generally impair the secretion of signaling molecules in peripheral glia. We expressed *UAS-sar1 RNAi* in perineurial glia using *Egr-Gal4* as well as *NP6293-Gal4* (Awasaki et al., 2008; Stork et al., 2012) and assayed PHP (Figure S5). First, we demonstrated that perineurial glia were normally distributed and were present at the NMJ when Sar1 was knocked down in perineurial glia, although there were changes in glial morphology at the NMJ (Figure S5F). Next, we demonstrated impaired basal

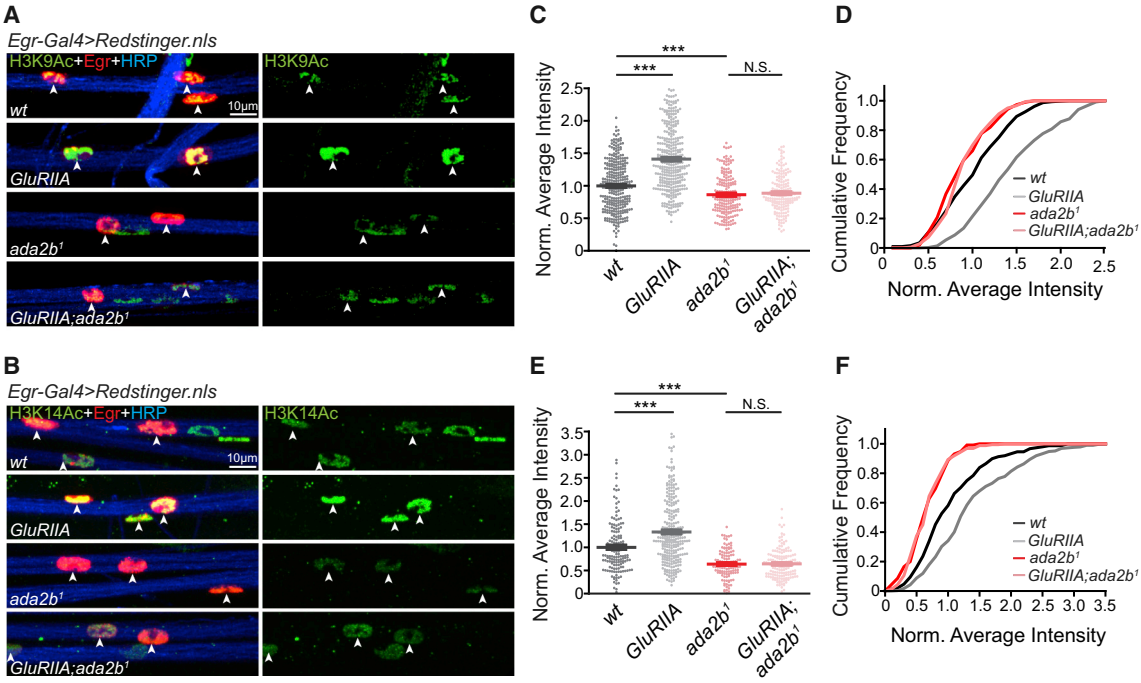

Figure 4. Glial H3K9Ac and H3K14Ac Are Enhanced in Egr Positive Cells in the *GluRIIA* Mutant

(A and B) Representative confocal images of acetylated H3K9 (H3K9Ac, A) and acetylated H3K14 (H3K14Ac, B) in glial nuclei on peripheral nerves. Acetylated H3K9 or H3K14 (H3K9/14Ac, green), Egr positive glial nuclei (*Egr-Gal4 > Redstinger.nls*, red), and neuronal membrane (HRP, blue) are shown for WT, *GluRIIA* mutants, *ada2b*^{1} mutants, and *GluRIIA;ada2b*^{1} double mutants.

(C and D) Quantification of average H3K9Ac fluorescence intensity (C) and cumulative distribution of average H3K9Ac intensity (D) within Egr positive glial nuclei. Average intensities for WT (n = 309 nuclei, N = 6 animals, black), *GluRIIA* mutants (*GluRIIA*, n = 349 nuclei, N = 6 animals, gray), *ada2b*^{1} mutants (*ada2b*^{1}, n = 188 nuclei, N = 4 animals, red), and *GluRIIA;ada2b*^{1} double mutants (*GluRIIA;ada2b*^{1}, n = 179 nuclei, N = 4 animals, light red) are normalized to WT values. Mean ± SEM; ***p < 0.001; N.S.; one-way ANOVA, Bonferroni's multiple comparison test.

(E and F) Quantification of average H3K14Ac fluorescence intensity (E) and cumulative distribution of average H3K14Ac intensity (F) within Egr positive glial nuclei. Average intensities for the WT (n = 148 nuclei, N = 4 animals, black), *GluRIIA* mutants (*GluRIIA*, n = 284 nuclei, N = 4 animals, gray), *ada2b*^{1} mutants (*ada2b*^{1}, n = 115 nuclei, N = 4 animals, red), and *GluRIIA;ada2b*^{1} double mutants (*GluRIIA;ada2b*^{1}, n = 160 nuclei, N = 4 animals, light red) are normalized to WT values. Mean ± SEM; ***p < 0.001; N.S. not significant; one-way ANOVA, Bonferroni's multiple comparison test.

See also Figure S4.

synaptic transmission (Figures S5B and S5E), highlighting a role for Sar1-mediated secretory trafficking in glia during the development or maintenance of presynaptic release at baseline. Finally, we demonstrated a complete block of PHP following application of PhTX to the NMJ, suggesting that secretory trafficking in peripheral glia was necessary for PHP (Figures S5B–S5E). As a control, we probed synapse morphology at the NMJ when expressing *UAS-sar1 RNAi* in glia (Figures S5F–S5I). Although there was a slight increase of bouton numbers at the NMJ of muscle 6/7 (abdominal segment 2), the total number of presynaptic active zones remains normal (Figures S5F–S5I). There are many caveats to this experiment, given the non-specific disruption of secretory trafficking. None-the-less, the data demonstrate a requirement for peripheral glia in neuromuscular PHP.

Multiplexin Is Secreted by Perineurial Glia and Is Required for PHP

There is reason to hypothesize that Multiplexin, a component of the extracellular matrix (ECM) that is necessary for PHP (Wang et al., 2014), could be derived from glia. Multiplexin is the homolog of mammalian Collagen XVIII and can be cleaved to produce a conserved, matrix-derived signaling molecule, referred to as a matrikine, named Endostatin (O'Reilly et al., 1997; Wang et al., 2014). Although Endostatin is essential for PHP, the tissue that secretes and deposits Multiplexin at the NMJ remains unknown. More specifically, we reported that when transgenic Endostatin was supplied by either the neuron or muscle cell, it was sufficient, in either case, to support PHP in a *multiplexin* mutant (Wang et al., 2014). But, in this experiment, an artificial signal peptide drives constitutive secretion of Endostatin from either nerve or muscle. The endogenous source of Multiplexin was never determined, a question that can only be addressed by tissue-specific depletion of Multiplexin. Furthermore, it remains unknown whether, or how, Multiplexin secretion is altered during PHP.

Recently, a transcriptome profiling study identified *Drosophila multiplexin* as a downstream target gene of the SAGA complex in the *Drosophila* visual system (Ma et al., 2016). Thus, we hypothesized that SAGA complex-dependent expression and secretion

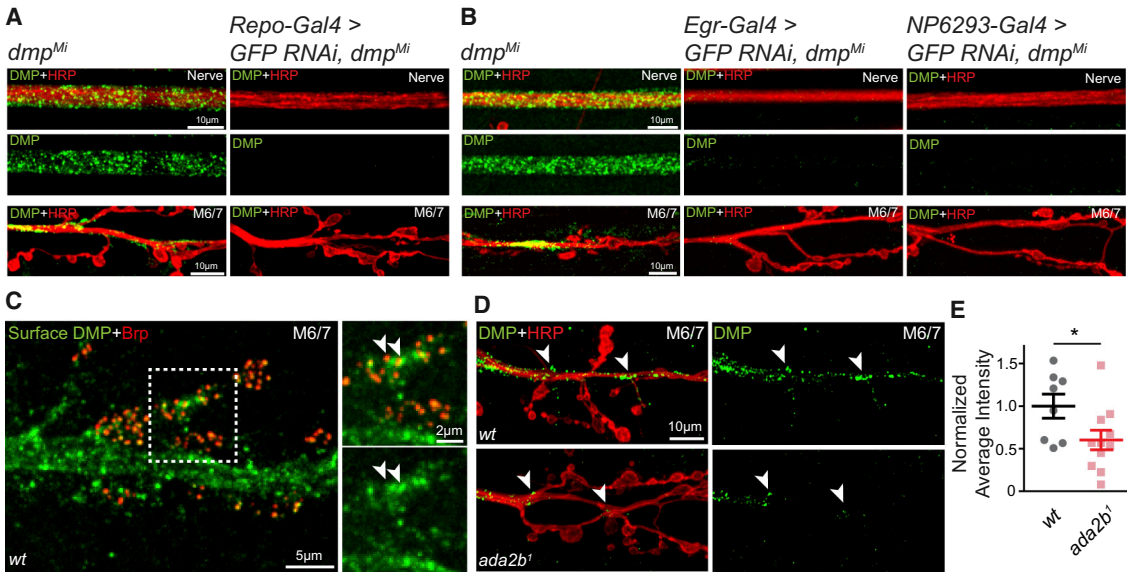

Figure 5. Ada2b-Dependent Expression of Multiplexin in Perineurial Glia

(A and B) Representative confocal images for Multiplexin expression on peripheral nerves (top panels) and at the NMJ of muscle 6/7 (bottom panels). Endogenous Multiplexin is labeled by the dmp^{Mi} protein trap (DMP, green). Peripheral nerves and the presynaptic membrane at the NMJ are immunolabeled with HRP (red). Multiplexin-GFP is greatly diminished when *UAS-GFP RNAi* is expressed in the dmp^{Mi} protein trap line using pan glial-specific *Gal4* drivers (A, *Repo-Gal4 > GFP RNAi, dmp*^{Mi}) or perineurial glial-specific *Gal4* drivers (B, *Egr-Gal4 > GFP RNAi, dmp*^{Mi}; *NP6293-Gal4 > GFP RNAi, dmp*^{Mi}) compared to the control (dmp^{Mi}).

(C) Representative confocal images for extracellular Multiplexin (surface DMP, green). Endogenous Multiplexin is secreted into the ECM and is present throughout the NMJ in proximity to active zones (white arrows, inset; Brp, red) in WT animals.

(D and E) Representative confocal images (D) and quantification (E) of average fluorescence intensity of Multiplexin-GFP (dmp^{Mi} , GFP signal indicated by white arrows) at the NMJ of WT (black, n = 8 NMJ, N = 3 animals) and $ada2b^{1}$ mutants ($ada2b^{1}$, red, n = 11 NMJ, N = 3 animals). Normalized average intensity is shown. Mean ± SEM; *p < 0.05; Student's t test.

See also Figures S5 and S6.

of Multiplexin within glia could be a primary mechanism involved in PHP. To test this hypothesis, we used two independent methodologies. First, we examined the endogenous expression pattern of Multiplexin using a Multiplexin protein-trap line harboring a Mimic-PT.GFSTF.0 inserted within the *multiplexin* locus (Nagarkar-Jaiswal et al., 2015). The Mimic-PT.GFSTF.0 cassette is inserted in an intron close to the 3′ end of the gene, and the GFP-tagged protein reports the endogenous expression of the Multiplexin protein. Multiplexin-tagged-GFP is observed in cells localized on the surface of the ventral nerve cord (data not shown) and in cells surrounding all peripheral nerves (Figure 5A). Multiplexin-GFP was also observed at the NMJ, consistent with the anatomical position of peripheral glia in axons and at the NMJ (Figures 5A and 5B). We then probed the co-localization of Multiplexin-GFP with perineurial and subperineurial glia (Figure S6). We visualized peripheral glia by expressing *UAS-tdTomato* using the *Egr-Gal4* driver and simultaneously visualized Multiplexin-GFP. Multiplexin-GFP shows precise co-localization with tdTomato expressing glia within the peripheral nerve and at the NMJ (Figures S6A and S6C). In contrast, when we drive the expression of *UAS-tdTomato* using subperineurial glial Gal4 driver *Moody-Gal4* (Schwabe et al., 2005; Stork et al., 2012), Multiplexin-GFP is concentrated in cells localized outside the subperineurial glial layer on the peripheral nerves, suggesting that Multiplexin is strongly expressed in perineurial glia in the periphery (Figure S6B).

As a second approach, we tested whether perineurial glia, identified by *Egr-Gal4* or *NP6293-Gal4*, are the sole source of Multiplexin. To do so, we selectively depleted the endogenously tagged Multiplexin-GFP protein in glia by expressing *UAS-GFP RNAi*. The *UAS-GFP RNAi* was expressed with a pan-glial-specific *Gal4* driver (*Repo-Gal4*; Sepp et al., 2001; Stork et al., 2012), as well as the two perineurial glia-specific *Gal4* drivers (*Egr-Gal4* and *NP6293-Gal4*). We found that Multiplexin-GFP was completely abolished, regardless of which *Gal4* driver was used (Figures 5A and 5B). Thus, Multiplexin protein that resides in peripheral nerve as well as at the NMJ is solely derived from the perineurial glia identified by *Egr-Gal4* or *NP6293-Gal4*.

Next, to complement the above analyses, we used non-cell-permeabilizing conditions to immunolabel Multiplexin, thereby testing the abundance of the secreted form of Multiplexin protein (Figure 5C). We previously demonstrated the specificity of our non-cell permeabilizing protocol (Wang et al., 2014). The Multiplexin antibody that we used recognizes the C-terminal Endostatin domain of Multiplexin (Harpaz et al., 2013). Antibody specificity was verified by the lack of signal in a *multiplexin*-null mutant and a C-terminal deletion mutant (data not shown). In our experiment, the NMJ was co-labeled for surface Endostatin (without permeabilization) and the active zone component Brp (after fixation and permeabilization, Figure 5C). This double-labeling protocol was also previously verified (Wang et al., 2014).

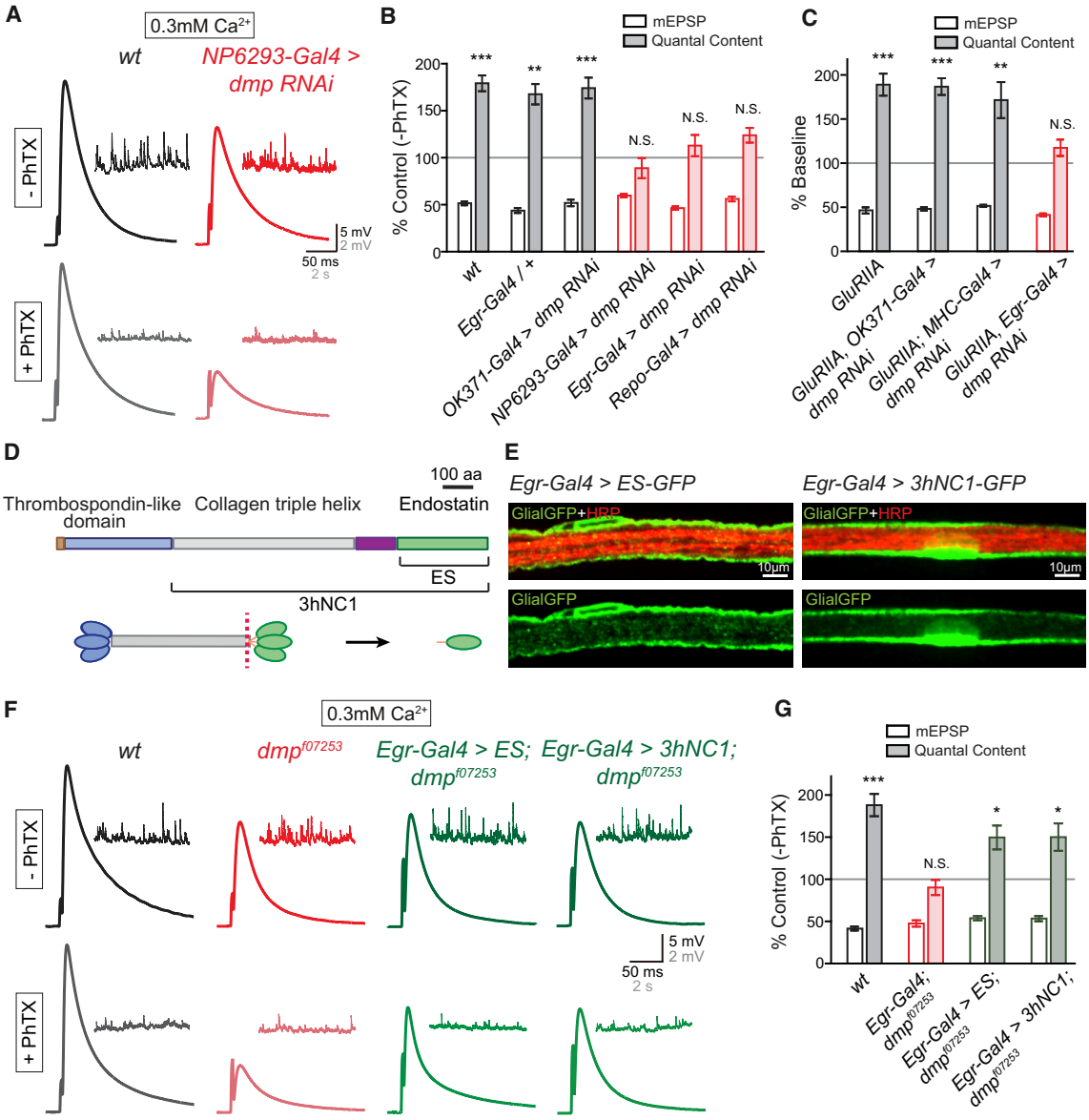

Figure 6. Glial-Derived Multiplexin Is Required for PHP

(A) Representative EPSP and mEPSP traces in WT (black) and at the NMJ when *UAS-dmp RNAi* is driven by the perineurial glial-specific *Gal4* driver *NP6293-Gal4* (red) in the absence (–PhTX) and the presence of PhTX (+PhTX).

(B) Percentage of change in mEPSP (open bars) and quantal content (filled bars) in the presence of PhTX, as in Figure 1C. Genotypes: WT (gray bars), synapses bearing heterozygous *Egr-Gal4* (*Egr-Gal4*/+, gray bars), *UAS-dmp RNAi* driven by motoneuron-specific *Gal4* (*OK371-Gal4 > dmp RNAi*, gray bars), *UAS-dmp RNAi* driven by perineurial glial-specific *Gal4* (*NP6293-Gal4 > dmp RNAi*, red), *UAS-dmp RNAi* driven by *Egr-Gal4* (*Egr-Gal4 > dmp RNAi*, red), and *UAS-dmp RNAi* driven by pan-glial *Gal4* (*Repo-Gal4 > dmp RNAi*, red bars). Mean ± SEM; **p < 0.01, ***p < 0.001, N.S.; Student's t test.

(C) Quantification of mEPSP (open) and quantal content (filled). Each genotype is presented as percentage of change due to the presence of the *GluRIIA* mutant. Genotypes: *GluRIIA* (*GluRIIA*, gray bars), *UAS-dmp RNAi* driven by motoneuron-specific *Gal4* in *GluRIIA* mutants (*GluRIIA, OK371-Gal4 > dmp RNAi*, gray bars), *UAS-dmp RNAi* driven by muscle-specific *Gal4* in *GluRIIA* (*GluRIIA; MHC-Gal4 > dmp RNAi*, gray bars), and *UAS-dmp RNAi* driven by glial-specific *Gal4* in *GluRIIA* (*GluRIIA, Egr-Gal4 > dmp RNAi*, red). Mean ± SEM; **p < 0.01, ***p < 0.001, N.S.; Student's t test.

(D) Diagram of the Multiplexin protein, the source of Endostatin. Thrombospondin-like domain (blue), Collagen triple helix (gray), and Endostatin domain (ES, green) of Multiplexin (top panel) are shown. Uncleaved middle-length isoform of Multiplexin (3hNC1) and cleaved form (Endostatin, abbreviated ES) are indicated. C-terminal domain of Multiplexin can be cleaved proteolytically (red dotted line, bottom panel) at hinge region to release monomers of Endostatin (ES, green oval).

(E) Representative confocal images of perineurial glia expressing *UAS-ES-GFP* (*Egr-Gal4>ES-GFP*, Glial-GFP, green, left panels) and *UAS-3hNC1-GFP* (*Egr-Gal4>3hNC1-GFP*, Glial-GFP, green, right panels) driven by *Egr-Gal4* on the peripheral nerve. Neuronal membrane is indicated by anti-HRP labeling (HRP, red).

(legend continued on next page)

We found that extracellular Multiplexin formed punctuate structures that were distributed throughout the presynaptic nerve terminal, and these structures were often present in close proximity to presynaptic active zones (Figure 5C). Thus, endogenous Multiplexin protein is secreted and is present at or in close proximity to neurotransmitter release sites.

Finally, we tested whether the abundance of Multiplexin protein, at the NMJ, was dependent upon SAGA complex function. We estimated total Multiplexin protein by staining for Multiplexin-GFP in the GFP protein trap (Mimic-PT.GFSTF.0; Figure 5D) using permeabilizing conditions. We found that synaptic Multiplexin-GFP is reduced by ~50% in the *ada2b*^{1} mutant compared to wild type (Figures 5D and 5E), demonstrating that Multiplexin protein levels were strongly influenced, but not completely dependent upon, the activity of *ada2b*. Thus, Ada2b is essential for PHP and controls the abundance of Multiplexin, a required PHP protein.

Perineurial Glia-Derived Multiplexin Is Required for PHP

We then determined whether glia are the relevant source of Multiplexin that is necessary for the rapid induction and sustained expression of PHP. We knocked down *multiplexin*, using *UAS-multiplexin RNAi*, and did so in either motoneurons (*OK371-Gal4*) or glia (using each of the following drivers individually: *Egr-Gal4*, *NP6293-Gal4*, or *Repo-Gal4*). We observed a complete block of synaptic homeostasis when we expressed *UAS-multiplexin RNAi* in glia using either pan-glial (*Repo-Gal4*) or when using either of the perineurial-specific glial (*NP6293-Gal4* and *Egr-Gal4*) drivers (Figures 6A, 6B, and S7). Note that, when *multiplexin* expression was knocked down in motoneurons, PHP was normal (Figures 6B and S7), a finding that effectively controls for the use of the RNAi line.

An identical dataset was collected using the *GluRIIA* mutant to induce PHP. We observed impaired homeostasis only when *multiplexin* was specifically depleted in glia (Figures 6C and S7). Finally, we complemented our tissue-specific RNAi experiments with tissue-specific genetic rescue. We expressed the full-length Multiplexin (*UAS-3hNC1*, Figure 6D) or the C-terminal Endostatin domain of Multiplexin (*UAS-ES*, Figure 6D; Meyer and Moussian, 2009) in the *multiplexin*-null mutant (*dmp*^{f07253}) using a peripheral glial-specific *Gal4* driver (*Egr-Gal4*). We observe a strong GFP signal when we drive the expression of *UAS-3hNC1-GFP* or *UAS-ES-GFP* using *Egr-Gal4*, demonstrating robust expression of these transgenes (Figure 6E). Glial-specific expression of *UAS-3hNC1* (*Egr-Gal4 > 3hNC1;dmp*^{f07253}) or *UAS-Endostatin* (*Egr-Gal4 > ES;dmp*^{f07253}) rescues PHP in the *multiplexin*-null mutant, whereas the heterozygous *Egr-Gal4* driver alone (*Egr-Gal4/+;dmp*^{f07253}) does not (Figures 6F and 6G). Based on these experiments, we conclude that peripheral glia, and perineurial glia more specifically, are the relevant source of Multiplexin protein, necessary for the both the rapid induction and sustained expression of PHP.

SAGA Mediates the Upregulation of Multiplexin in the *GluRIIA* Mutant

As a final set of experiments, we asked whether Multiplexin transcript and protein were modulated during the long-term expression of PHP, caused by the *GluRIIA* mutation and whether this modulation was sensitive to SAGA mutations. First, we demonstrated an ~50% increase of Multiplexin protein expression at the NMJ of the *GluRIIA* mutant compared to wild type (Figures 7A, 7B, and 7E). To our surprise, we also observed a widespread increase in Multiplexin (Figures 7C–7E) that correlates with the wide-spread changes in Ada2b-dependent histone acetylation within peripheral glia in the *GluRIIA* mutant background (Figures 4A–4F). Next, we extended this observation by demonstrating an ~100% increase of *multiplexin* mRNA level in the *GluRIIA* mutant larval brain compared to wild type (Figure 7F). As predicted, the increase in *multiplexin* mRNA is restored to baseline levels in the *GluRIIA;ada2b*^{EP} double mutant, indicating that the elevated *multiplexin* gene expression is Ada2b dependent. Since the *ada2b* allele used in this experiment (*ada2b*^{EP}) also blocks PHP in the *GluRIIA* mutant background (Figure S8), it argues that Ada2b-dependent modulation of *multiplexin* expression and protein are linked to the expression of PHP.

Finally, we address whether Multiplexin is the only glial-derived signal that is important for PHP. In other words, is SAGA-dependent modulation of Multiplexin sufficient to explain the entire glia and SAGA-dependent control of PHP? We hypothesize that Multiplexin is, actually, only one component of a more complex SAGA and glial-specific signaling event. Indeed, glial-specific expression of a secreted form of Endostatin that is sufficient to rescue the *multiplexin* mutant (Figures 6F and 6G) fails to restore PHP in the *ada2b*^{1} mutant (Figures 7G–7J).

DISCUSSION

Based on our accumulated data, we propose the existence of a previously unexplored homeostatic signaling system, originating in muscle following perturbation of muscle-specific glutamate receptors. This muscle-derived signal, of unknown identity, activates SAGA-dependent epigenetic changes that occur throughout glial cells in the peripheral nerves, both within the nerves themselves and in close proximity to the neuromuscular active zones. The glial epigenetic signaling response is essential for PHP, as demonstrated by the required function of four new PHP genes, all components of the SAGA complex.

(F) Representative EPSP and mEPSP traces in WT (black), *multiplexin* mutants (*dmp*^{f07253}, red), *UAS-ES* driven by *Egr-Gal4* in *dmp*^{f07253} mutants (*Egr-Gal4 > ES;dmp*^{f07253}, green), and *UAS-3hNC1* driven by *Egr-Gal4* in *dmp*^{f07253} mutants (*Egr-Gal4 > 3hNC1;dmp*^{f07253}, green) in the absence (–PhTX) and presence of philanthotoxin (+PhTX).

(G) Quantification of mEPSP amplitude (open bars) and quantal content (filled bars), normalized as in (B). Genotypes: WT (gray bars), *dmp*^{f07253} mutants bearing heterozygous *Egr-Gal4* (*Egr-Gal4/+;dmp*^{f07253}, red bars), *UAS-ES* driven by *Egr-Gal4* in *dmp*^{f07253} mutant (*Egr-Gal4 > UAS-ES;dmp*^{f07253}, green bars), and *UAS-3hNC1* driven by *Egr-Gal4* in *dmp*^{f07253} mutant (*Egr-Gal4 > UAS-3hNC1;dmp*^{f07253}, green bars).

Mean ± SEM; *p < 0.05, ***p < 0.001, N.S. not significant; Student's t test.

See also Figure S7.

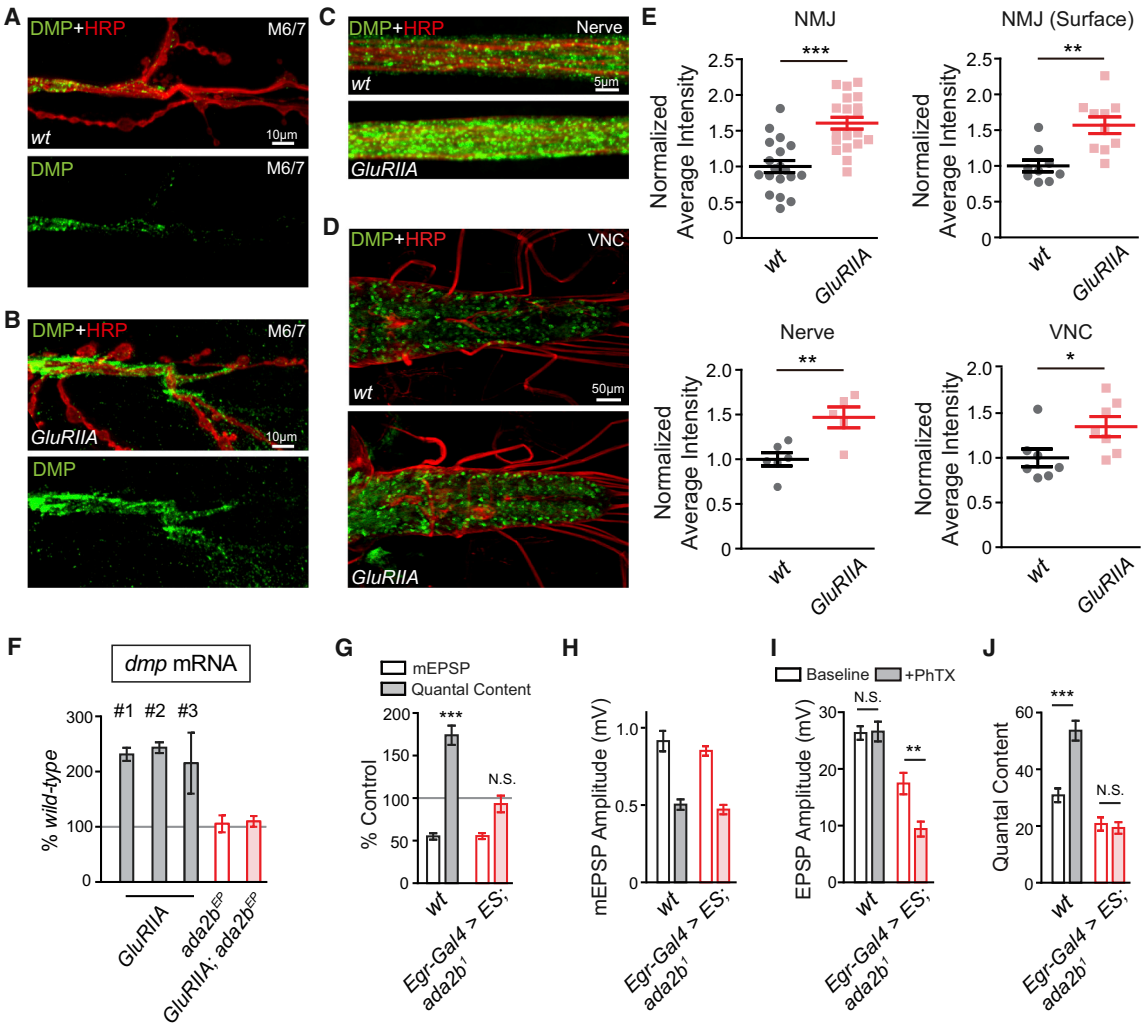

Figure 7. SAGA-Dependent Enhancement of Peripheral Multiplexin Expression during Homeostatic Plasticity

(A–D) Representative confocal images of Multiplexin protein at the NMJ on muscle 6/7 (A) and (B), the peripheral nerve (C, nerve), and the ventral nerve cord (D, VNC) in WT and *GluRIIA* mutants. Total endogenous Multiplexin is labeled by dmp^{Mi} protein trap (DMP, green), and the neuronal membrane is indicated by anti-HRP immunolabeling (HRP, red).

(E) Quantification of average fluorescence intensity of total endogenous Multiplexin at the NMJ (NMJ, WT n = 19 synapses, N = 7 animals; *GluRIIA* n = 20 synapses, N = 7 animals), on the peripheral nerve (nerve, WT N = 6 animals; *GluRIIA* N = 5 animals) and in the VNC (VNC, WT N = 7 animals; *GluRIIA* N = 7 animals) in the WT control and *GluRIIA* mutant animals. The average fluorescence intensity of extracellular endogenous Multiplexin is quantified at the NMJ (NMJ surface, WT n = 9 synapses, N = 3 animals; *GluRIIA* n = 10 synapses, N = 3 animals) in WT and *GluRIIA* mutants. Mean ± SEM; *p < 0.05; **p < 0.01; ***p < 0.001; Student's t test.

(F) Quantification of *dmp* mRNA level by qPCR. The *dmp* transcript levels in *GluRIIA* (three independent measures, #1 - #3), $ada2b^{EP}$ mutant ($ada2b^{EP}$, red empty bar), and *GluRIIA*;$ada2b^{EP}$ double mutants (*GluRIIA*;$ada2b^{EP}$, red filled bar) are normalized to WT values.

(G) mEPSP amplitudes (open bars) and quantal content (filled bars) recorded in PhTX and normalized to each genotype in the absence of PhTX. Genotypes: WT (gray bars) and *UAS-ES* driven by *Egr-Gal4* in $ada2b^{1}$ mutant (*Egr-Gal4 > ES*,$ada2b^{1}$, red bars). Mean ± SEM; ***p < 0.001, N.S.; Student's t test.

(H–J) Non-normalized values in the absence (open bars) and presence (filled bars) of PhTX for mEPSP amplitude (H), EPSP amplitude (I) and quantal content (J). Mean ± SEM; **p < 0.01***p < 0.001, N.S. not significant; Student's t test.

See also Figure S8.

We provide evidence that one element of the SAGA-dependent epigenetic signaling is enhanced deposition of the ECM protein Multiplexin, a required factor for both short and long-term PHP. We hypothesize that this represents a stable change of ECM composition that sustains a homeostatic change in motor function (Figure 8).

Role of the ECM

We demonstrate enhanced deposition of Multiplexin in the *GluRIIA* mutant background that is Ada2b dependent and correlates with increased histone acetylation throughout peripheral glia. Remarkably, elevated Multiplexin is not restricted to the NMJ, or even to the peripheral nerves. This is evidence of a

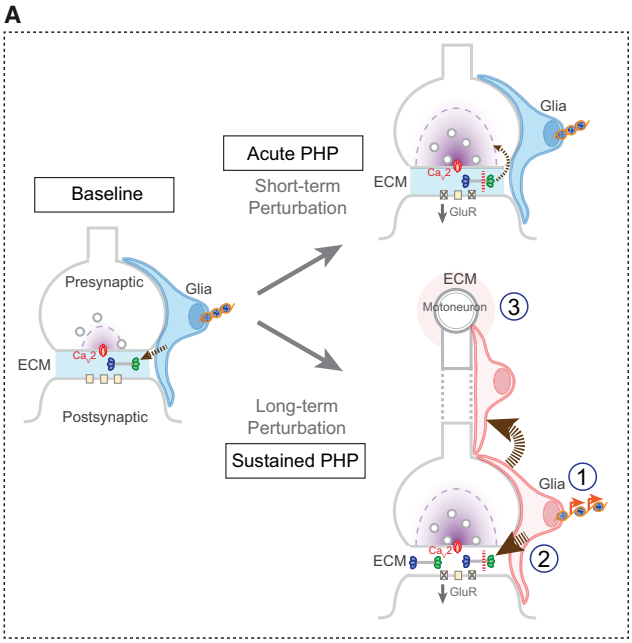

Figure 8. Model for Glia Signaling in PHP

The SAGA complex is required for both the rapid induction and sustained expression of PHP. At baseline, glial secrete Multiplexin, which is deposited within the extracellular matrix (ECM) at the NMJ (arrow, left panel). Application of PhTX (short-term perturbation) results in the proteolytic cleavage of Multiplexin and the release of Endostatin, which is essential for the induction of PHP (acute PHP, top-right panel). A sustained perturbation (long-term perturbation), such as the *GluRIIA* mutation, induces epigenetic signaling in peripheral glia, a process that is necessary for the sustained expression of PHP (bottom-right panel). Within peripheral glia, members of the SAGA complex are required for secretion of elevated levels of Multiplexin and other, as-yet-unidentified, factors that function either locally (1), along the peripheral nerve (2), or within the ventral nerve cord where the motoneuron cell bodies reside (3).

systemic response, affecting the entirety of the peripheral nerve and ventral nerve cord, in response to the muscle-specific deletion of a non-essential glutamate receptor subunit, GluRIIA. Many possibilities exist for this systemic response. It certainly implies the existence of a homeostatic signaling from muscle to glia. But, it also argues that this signal is broadly released and diffusible or is a signal that can be propagated through glial-glial junctions (Figure 8), originating at the NMJ and extending throughout the peripheral nerves. Finally, another possibility is that signaling from muscle to nerve (Orr et al., 2017) could induce secondary signaling from the motoneurons to surrounding glia, with glia mediating feedback signaling including the deposition of increased levels of Multiplexin (Figure 8).

Why is there a systemic response? There exists precedent for dynamic epigenetic signaling in the nervous system, including the molecular mechanisms that control circadian rhythm (Aguilar-Arnal and Sassone-Corsi, 2015; Etchegaray et al., 2003; Koike et al., 2012). One possibility is that the spread of the Multiplexin signal throughout the periphery, extending to the CNS, might be preparatory for additional perturbations. For example, if a perturbation was to be environmental, immunological, or injury related, as opposed to muscle-specific elimination of a glutamate receptor, then it might be advantageous to prepare surrounding tissue for the eventual spread of such a persistent perturbation. This is speculative but is consistent with theoretical models of homeostasis, adaptation, resilience, and allostasis in other systems (Karatsoreos and McEwen, 2011). We also note the formal possibility that a systemic response could be initiated centrally and propagate to the periphery, something that could be addressed in the future.

There is yet another possibility. The systemic remodeling of the ECM could influence the induction of Hebbian-type plasticity within the CNS following disruption of transmission at the NMJ. In the mammalian CNS, glia and ECM structures surrounding neurons control synaptic transmission, neuron excitability, and neuronal states (Poskanzer and Yuste, 2016; Sorg et al., 2016; Volterra and Meldolesi, 2005; Wang and Fawcett, 2012). Previous studies demonstrated that the ECM remodeling can be induced by synaptic signals and ECM signaling influences the expression of Hebbian synaptic plasticity (Dityatev and Schachner, 2003; Tonnesen et al., 2018). These are testable possibilities for future studies.

Epigenetic Signaling, Homeostatic Plasticity, and Etiology of Disease

There is an emerging literature regarding epigenetic regulation of gene expression during Hebbian plasticity (Gräff and Tsai, 2013; Levenson and Sweatt, 2005), although a glial-specific function is lacking. By contrast, very little is known about the function and capacity of epigenetic codes during homeostatic plasticity. And, virtually nothing is known about how the glial epigenome maintains the stability and function of the nervous system. Mutations in epigenetic factors or abnormal epigenetic modifications have been associated with numerous neurodevelopmental, neuropsychiatric, and neurodegenerative disorders (Chen et al., 2003, 2012; De Rubeis et al., 2014). In most instances, including autism spectrum disorder, the focus remains on direct effects within neurons and at specific time points during neurodevelopment (Willsey et al., 2013). The importance of these data is emphasized by reports documenting remarkable benefit from histone deacetylase (HDAC) inhibitors in clinical settings (Fischer et al., 2007; Steffan et al., 2001), but the locus of action (neuron versus glia) remains to be defined. Importantly, there are data for Rett syndrome indicating a loss of epigenetic control within glia (Lioy et al., 2011). Our results not only emphasize the need for further exploration of glial-dependent epigenetic signaling in neurological and psychiatric disease but set the stage for determining whether glial-derived epigenetic signaling may be a cellular and molecular link that connects homeostatic plasticity to these devastating disorders.

STAR★METHODS

Detailed methods are provided in the online version of this paper and include the following:

- KEY RESOURCES TABLE
- LEAD CONTACT AND MATERIALS AVAILABILITY
- EXPERIMENTAL MODEL AND SUBJECT DETAILS
- METHOD DETAILS
  - Electrophysiology
  - Immunocytochemistry

SUPPLEMENTAL INFORMATION

Supplemental Information can be found online at https://doi.org/10.1016/j.neuron.2019.10.041.

ACKNOWLEDGMENTS

Work in the laboratory of G.W.D. was supported by NIH NINDS, U.S.A. grant R35-NS097212. T.W. was supported by NIH NRSA postdoc fellowship NINDS, U.S.A. 1F32NS081884-03.

AUTHOR CONTRIBUTIONS

Project Design, Data Collection, Data Analysis, Interpretation, and Manuscript Co-writing and Editing, T.W.; Data Collection and Analysis, D.T.M. and N.H.; Project Design, Data Interpretation, and Manuscript Writing, G.W.D.

DECLARATION OF INTERESTS

The authors declare no competing interests.

Received: June 22, 2018
Revised: August 30, 2019
Accepted: October 29, 2019
Published: December 3, 2019

REFERENCES

Aguilar-Arnal, L., and Sassone-Corsi, P. (2015). Chromatin landscape and circadian dynamics: Spatial and temporal organization of clock transcription. Proc. Natl. Acad. Sci. USA *112*, 6863–6870.

Amir, R.E., Van den Veyver, I.B., Wan, M., Tran, C.Q., Francke, U., and Zoghbi, H.Y. (1999). Rett syndrome is caused by mutations in X-linked MECP2, encoding methyl-CpG-binding protein 2. Nat. Genet. *23*, 185–188.

Arthur-Farraj, P.J., Morgan, C.C., Adamowicz, M., Gomez-Sanchez, J.A., Fazal, S.V., Beucher, A., Razzaghi, B., Mirsky, R., Jessen, K.R., and Aitman, T.J. (2017). Changes in the Coding and Non-coding Transcriptome and DNA Methylome that Define the Schwann Cell Repair Phenotype after Nerve Injury. Cell Rep. *20*, 2719–2734.

Awasaki, T., Lai, S.L., Ito, K., and Lee, T. (2008). Organization and postembryonic development of glial cells in the adult central brain of Drosophila. J. Neurosci. *28*, 13742–13753.

Baizabal, J.M., Mistry, M., Garcia, M.T., Gomez, N., Olukoya, O., Tran, D., Johnson, M.B., Walsh, C.A., and Harwell, C.C. (2018). The epigenetic state of PRDM16-regulated enhancers in radial glia controls cortical neuron position. Neuron *98*, 945–962.

Beattie, E.C., Stellwagen, D., Morishita, W., Bresnahan, J.C., Ha, B.K., Von Zastrow, M., Beattie, M.S., and Malenka, R.C. (2002). Control of synaptic strength by glial TNFalpha. Science *295*, 2282–2285.

Benevento, M., Iacono, G., Selten, M., Ba, W., Oudakker, A., Frega, M., Keller, J., Mancini, R., Lewerissa, E., Kleefstra, T., et al. (2016). Histone Methylation by the Kleefstra Syndrome Protein EHMT1 Mediates Homeostatic Synaptic Scaling. Neuron *91*, 341–355.

Bergquist, S., Dickman, D.K., and Davis, G.W. (2010). A hierarchy of cell intrinsic and target-derived homeostatic signaling. Neuron *66*, 220–234.

Blackman, M.P., Djukic, B., Nelson, S.B., and Turrigiano, G.G. (2012). A critical and cell-autonomous role for MeCP2 in synaptic scaling up. J. Neurosci. *32*, 13529–13536.

Brink, D.L., Gilbert, M., Xie, X., Petley-Ragan, L., and Auld, V.J. (2012). Glial processes at the Drosophila larval neuromuscular junction match synaptic growth. PLoS ONE *7*, e37876.

Carré, C., Szymczak, D., Pidoux, J., and Antoniewski, C. (2005). The histone H3 acetylase dGcn5 is a key player in Drosophila melanogaster metamorphosis. Mol. Cell. Biol. *25*, 8228–8238.

Chen, W.G., Chang, Q., Lin, Y., Meissner, A., West, A.E., Griffith, E.C., Jaenisch, R., and Greenberg, M.E. (2003). Derepression of BDNF transcription involves calcium-dependent phosphorylation of MeCP2. Science *302*, 885–889.

Chen, Y.C., Gatchel, J.R., Lewis, R.W., Mao, C.A., Grant, P.A., Zoghbi, H.Y., and Dent, S.Y. (2012). Gcn5 loss-of-function accelerates cerebellar and retinal degeneration in a SCA7 mouse model. Hum. Mol. Genet. *21*, 394–405.

Christopherson, K.S., Ullian, E.M., Stokes, C.C., Mullowney, C.E., Hell, J.W., Agah, A., Lawler, J., Mosher, D.F., Bornstein, P., and Barres, B.A. (2005). Thrombospondins are astrocyte-secreted proteins that promote CNS synaptogenesis. Cell *120*, 421–433.

Coffee, B., Zhang, F., Warren, S.T., and Reines, D. (1999). Acetylated histones are associated with FMR1 in normal but not fragile X-syndrome cells. Nat. Genet. *22*, 98–101.

Cull-Candy, S.G., Miledi, R., Trautmann, A., and Uchitel, O.D. (1980). On the release of transmitter at normal, myasthenia gravis and myasthenic syndrome affected human end-plates. J. Physiol. *299*, 621–638.

Davis, G.W. (2013). Homeostatic signaling and the stabilization of neural function. Neuron *80*, 718–728.

Davis, G.W., and Müller, M. (2015). Homeostatic control of presynaptic neurotransmitter release. Annu. Rev. Physiol. *77*, 251–270.

De Rubeis, S., He, X., Goldberg, A.P., Poultney, C.S., Samocha, K., Cicek, A.E., Kou, Y., Liu, L., Fromer, M., Walker, S., et al.; DDD Study; Homozygosity Mapping Collaborative for Autism; UK10K Consortium (2014). Synaptic, transcriptional and chromatin genes disrupted in autism. Nature *515*, 209–215.

Dityatev, A., and Schachner, M. (2003). Extracellular matrix molecules and synaptic plasticity. Nat. Rev. Neurosci. *4*, 456–468.

Doherty, J., Logan, M.A., Taşdemir, O.E., and Freeman, M.R. (2009). Ensheathing glia function as phagocytes in the adult Drosophila brain. J. Neurosci. *29*, 4768–4781.

Eroglu, C., Allen, N.J., Susman, M.W., O'Rourke, N.A., Park, C.Y., Ozkan, E., Chakraborty, C., Mulinyawe, S.B., Annis, D.S., Huberman, A.D., et al. (2009). Gabapentin receptor alpha2delta-1 is a neuronal thrombospondin receptor responsible for excitatory CNS synaptogenesis. Cell *139*, 380–392.

Etchegaray, J.P., Lee, C., Wade, P.A., and Reppert, S.M. (2003). Rhythmic histone acetylation underlies transcription in the mammalian circadian clock. Nature *421*, 177–182.

Fischer, A., Sananbenesi, F., Wang, X., Dobbin, M., and Tsai, L.H. (2007). Recovery of learning and memory is associated with chromatin remodelling. Nature *447*, 178–182.

Frank, C.A., Kennedy, M.J., Goold, C.P., Marek, K.W., and Davis, G.W. (2006). Mechanisms underlying the rapid induction and sustained expression of synaptic homeostasis. Neuron *52*, 663–677.

Frank, C.A., Pielage, J., and Davis, G.W. (2009). A presynaptic homeostatic signaling system composed of the Eph receptor, ephexin, Cdc42, and CaV2.1 calcium channels. Neuron *61*, 556–569.

Gaviño, M.A., Ford, K.J., Archila, S., and Davis, G.W. (2015). Homeostatic synaptic depression is achieved through a regulated decrease in presynaptic calcium channel abundance. eLife *4*. Published online April 17, 2015. https://doi.org/10.7554/eLife.05473.

Gräff, J., and Tsai, L.H. (2013). Histone acetylation: molecular mnemonics on the chromatin. Nat. Rev. Neurosci. *14*, 97–111.

Guzman-Karlsson, M.C., Meadows, J.P., Gavin, C.F., Hablitz, J.J., and Sweatt, J.D. (2014). Transcriptional and epigenetic regulation of Hebbian and non-Hebbian plasticity. Neuropharmacology *80*, 3–17.

Harpaz, N., Ordan, E., Ocorr, K., Bodmer, R., and Volk, T. (2013). Multiplexin promotes heart but not aorta morphogenesis by polarized enhancement of slit/robo activity at the heart lumen. PLoS Genet. *9*, e1003597.

Hauswirth, A.G., Ford, K.J., Wang, T., Fetter, R.D., Tong, A., and Davis, G.W. (2018). A postsynaptic PI3K-cII dependent signaling controller for presynaptic homeostatic plasticity. eLife *7*. Published online January 5, 2018. https://doi.org/10.7554/eLife.31535.

Helmlinger, D., and Tora, L. (2017). Sharing the SAGA. Trends Biochem. Sci. *42*, 850–861.

Hong, S., Beja-Glasser, V.F., Nfonoyim, B.M., Frouin, A., Li, S., Ramakrishnan, S., Merry, K.M., Shi, Q., Rosenthal, A., Barres, B.A., et al. (2016). Complement and microglia mediate early synapse loss in Alzheimer mouse models. Science *352*, 712–716.

Jimenez-Pacheco, A., Franco, J.M., Lopez, S., Gomez-Zumaquero, J.M., Magdalena Leal-Lasarte, M., Caballero-Hernandez, D.E., Cejudo-Guillén, M., and Pozo, D. (2017). Epigenetic Mechanisms of Gene Regulation in Amyotrophic Lateral Sclerosis. Adv. Exp. Med. Biol. *978*, 255–275.

Karatsoreos, I.N., and McEwen, B.S. (2011). Psychobiological allostasis: resistance, resilience and vulnerability. Trends Cogn. Sci. *15*, 576–584.

Keller, L.C., Cheng, L., Locke, C.J., Müller, M., Fetter, R.D., and Davis, G.W. (2011). Glial-derived prodegenerative signaling in the Drosophila neuromuscular system. Neuron *72*, 760–775.

Kerr, K.S., Fuentes-Medel, Y., Brewer, C., Barria, R., Ashley, J., Abruzzi, K.C., Sheehan, A., Tasdemir-Yilmaz, O.E., Freeman, M.R., and Budnik, V. (2014). Glial wingless/Wnt regulates glutamate receptor clustering and synaptic physiology at the Drosophila neuromuscular junction. J. Neurosci. *34*, 2910–2920.

Koike, N., Yoo, S.H., Huang, H.C., Kumar, V., Lee, C., Kim, T.K., and Takahashi, J.S. (2012). Transcriptional architecture and chromatin landscape of the core circadian clock in mammals. Science *338*, 349–354.

Koreman, E., Sun, X., and Lu, Q.R. (2018). Chromatin remodeling and epigenetic regulation of oligodendrocyte myelination and myelin repair. Mol. Cell. Neurosci. *87*, 18–26.

Lee, K.K., and Workman, J.L. (2007). Histone acetyltransferase complexes: one size doesn't fit all. Nat. Rev. Mol. Cell Biol. *8*, 284–295.

Levenson, J.M., and Sweatt, J.D. (2005). Epigenetic mechanisms in memory formation. Nat. Rev. Neurosci. *6*, 108–118.

Lindblad, K., Savontaus, M.L., Stevanin, G., Holmberg, M., Digre, K., Zander, C., Ehrsson, H., David, G., Benomar, A., Nikoskelainen, E., et al. (1996). An expanded CAG repeat sequence in spinocerebellar ataxia type 7. Genome Res. *6*, 965–971.

Lioy, D.T., Garg, S.K., Monaghan, C.E., Raber, J., Foust, K.D., Kaspar, B.K., Hirrlinger, P.G., Kirchhoff, F., Bissonnette, J.M., Ballas, N., and Mandel, G. (2011). A role for glia in the progression of Rett's syndrome. Nature *475*, 497–500.

Ma, J., Brennan, K.J., D'Aloia, M.R., Pascuzzi, P.E., and Weake, V.M. (2016). Transcriptome Profiling Identifies Multiplexin as a Target of SAGA Deubiquitinase Activity in Glia Required for Precise Axon Guidance During Drosophila Visual Development. G3 (Bethesda) *6*, 2435–2445.

Mahoney, R.E., Rawson, J.M., and Eaton, B.A. (2014). An age-dependent change in the set point of synaptic homeostasis. J. Neurosci. *34*, 2111–2119.

Marie, B., Sweeney, S.T., Poskanzer, K.E., Roos, J., Kelly, R.B., and Davis, G.W. (2004). Dap160/intersectin scaffolds the periactive zone to achieve high-fidelity endocytosis and normal synaptic growth. Neuron *43*, 207–219.

Meadows, J.P., Guzman-Karlsson, M.C., Phillips, S., Holleman, C., Posey, J.L., Day, J.J., Hablitz, J.J., and Sweatt, J.D. (2015). DNA methylation regulates neuronal glutamatergic synaptic scaling. Sci. Signal. *8*, ra61.

Meyer, F., and Moussian, B. (2009). Drosophila multiplexin (Dmp) modulates motor axon pathfinding accuracy. Dev. Growth Differ. *51*, 483–498.

Müller, M., Liu, K.S., Sigrist, S.J., and Davis, G.W. (2012). RIM controls homeostatic plasticity through modulation of the readily-releasable vesicle pool. J. Neurosci. *32*, 16574–16585.

Nagarkar-Jaiswal, S., DeLuca, S.Z., Lee, P.T., Lin, W.W., Pan, H., Zuo, Z., Lv, J., Spradling, A.C., and Bellen, H.J. (2015). A genetic toolkit for tagging intronic MiMIC containing genes. eLife *4*. Published online June 23, 2015. https://doi.org/10.7554/eLife.08469.

O'Reilly, M.S., Boehm, T., Shing, Y., Fukai, N., Vasios, G., Lane, W.S., Flynn, E., Birkhead, J.R., Olsen, B.R., and Folkman, J. (1997). Endostatin: an endogenous inhibitor of angiogenesis and tumor growth. Cell *88*, 277–285.

Orr, B.O., Fetter, R.D., and Davis, G.W. (2017). Retrograde semaphorin-plexin signalling drives homeostatic synaptic plasticity. Nature *550*, 109–113.

Petersen, S.A., Fetter, R.D., Noordermeer, J.N., Goodman, C.S., and DiAntonio, A. (1997). Genetic analysis of glutamate receptors in Drosophila reveals a retrograde signal regulating presynaptic transmitter release. Neuron *19*, 1237–1248.

Plomp, J.J., van Kempen, G.T., and Molenaar, P.C. (1992). Adaptation of quantal content to decreased postsynaptic sensitivity at single endplates in alpha-bungarotoxin-treated rats. J. Physiol. *458*, 487–499.

Poskanzer, K.E., and Yuste, R. (2016). Astrocytes regulate cortical state switching in vivo. Proc. Natl. Acad. Sci. USA *113*, E2675–E2684.

Qi, D., Larsson, J., and Mannervik, M. (2004). Drosophila Ada2b is required for viability and normal histone H3 acetylation. Mol. Cell. Biol. *24*, 8080–8089.

Schwabe, T., Bainton, R.J., Fetter, R.D., Heberlein, U., and Gaul, U. (2005). GPCR signaling is required for blood-brain barrier formation in Drosophila. Cell *123*, 133–144.

Sepp, K.J., Schulte, J., and Auld, V.J. (2001). Peripheral glia direct axon guidance across the CNS/PNS transition zone. Dev. Biol. *238*, 47–63.

Singh, S.K., Stogsdill, J.A., Pulimood, N.S., Dingsdale, H., Kim, Y.H., Pilaz, L.J., Kim, I.H., Manhaes, A.C., Rodrigues, W.S., Jr., Pamukcu, A., et al. (2016). Astrocytes Assemble Thalamocortical Synapses by Bridging NRX1α and NL1 via Hevin. Cell *164*, 183–196.

Sorg, B.A., Berretta, S., Blacktop, J.M., Fawcett, J.W., Kitagawa, H., Kwok, J.C., and Miquel, M. (2016). Casting a Wide Net: Role of Perineuronal Nets in Neural Plasticity. J. Neurosci. *36*, 11459–11468.

Staszewski, O., and Prinz, M. (2014). Glial epigenetics in neuroinflammation and neurodegeneration. Cell Tissue Res. *356*, 609–616.

Steffan, J.S., Bodai, L., Pallos, J., Poelman, M., McCampbell, A., Apostol, B.L., Kazantsev, A., Schmidt, E., Zhu, Y.Z., Greenwald, M., et al. (2001). Histone deacetylase inhibitors arrest polyglutamine-dependent neurodegeneration in Drosophila. Nature *413*, 739–743.

Stellwagen, D., and Malenka, R.C. (2006). Synaptic scaling mediated by glial TNF-alpha. Nature *440*, 1054–1059.

Stevens, B., Allen, N.J., Vazquez, L.E., Howell, G.R., Christopherson, K.S., Nouri, N., Micheva, K.D., Mehalow, A.K., Huberman, A.D., Stafford, B., et al. (2007). The classical complement cascade mediates CNS synapse elimination. Cell *131*, 1164–1178.

Stogsdill, J.A., Ramirez, J., Liu, D., Kim, Y.H., Baldwin, K.T., Enustun, E., Ejikeme, T., Ji, R.R., and Eroglu, C. (2017). Astrocytic neuroligins control astrocyte morphogenesis and synaptogenesis. Nature *551*, 192–197.

Stork, T., Bernardos, R., and Freeman, M.R. (2012). Analysis of glial cell development and function in Drosophila. Cold Spring Harb. Protoc. *2012*, 1–17.

Sun, W., Poschmann, J., Cruz-Herrera Del Rosario, R., Parikshak, N.N., Hajan, H.S., Kumar, V., Ramasamy, R., Belgard, T.G., Elanggovan, B., Wong, C.C.Y., et al. (2016). Histone Acetylome-wide Association Study of Autism Spectrum Disorder. Cell *167*, 1385–1397.

Tonnesen, J., Inavalli, V., and Nagerl, U.V. (2018). Super-Resolution Imaging of the Extracellular Space in Living Brain Tissue. Cell *172*, 1108–1121.

Tsankova, N., Renthal, W., Kumar, A., and Nestler, E.J. (2007). Epigenetic regulation in psychiatric disorders. Nat. Rev. Neurosci. *8*, 355–367.

Volterra, A., and Meldolesi, J. (2005). Astrocytes, from brain glue to communication elements: the revolution continues. Nat. Rev. Neurosci. *6*, 626–640.

Wang, D., and Fawcett, J. (2012). The perineuronal net and the control of CNS plasticity. Cell Tissue Res. *349*, 147–160.

Wang, T., Hauswirth, A.G., Tong, A., Dickman, D.K., and Davis, G.W. (2014). Endostatin is a trans-synaptic signal for homeostatic synaptic plasticity. Neuron *83*, 616–629.

Weake, V.M., and Workman, J.L. (2012). SAGA function in tissue-specific gene expression. Trends Cell Biol. *22*, 177–184.

Weake, V.M., Lee, K.K., Guelman, S., Lin, C.H., Seidel, C., Abmayr, S.M., and Workman, J.L. (2008). SAGA-mediated H2B deubiquitination controls the development of neuronal connectivity in the Drosophila visual system. EMBO J. *27*, 394–405.

Willsey, A.J., Sanders, S.J., Li, M., Dong, S., Tebbenkamp, A.T., Muhle, R.A., Reilly, S.K., Lin, L., Fertuzinhos, S., Miller, J.A., et al. (2013). Coexpression networks implicate human midfetal deep cortical projection neurons in the pathogenesis of autism. Cell *155*, 997–1007.

Yao, B., Christian, K.M., He, C., Jin, P., Ming, G.L., and Song, H. (2016). Epigenetic mechanisms in neurogenesis. Nat. Rev. Neurosci. *17*, 537–549.

Ye, B., Zhang, Y., Song, W., Younger, S.H., Jan, L.Y., and Jan, Y.N. (2007). Growing dendrites and axons differ in their reliance on the secretory pathway. Cell *130*, 717–729.

Younger, M.A., Müller, M., Tong, A., Pym, E.C., and Davis, G.W. (2013). A presynaptic ENaC channel drives homeostatic plasticity. Neuron *79*, 1183–1196.

Yu, H., Su, Y., Shin, J., Zhong, C., Guo, J.U., Weng, Y.L., Gao, F., Geschwind, D.H., Coppola, G., Ming, G.L., and Song, H. (2015). Tet3 regulates synaptic transmission and homeostatic plasticity via DNA oxidation and repair. Nat. Neurosci. *18*, 836–843.

STAR★METHODS

KEY RESOURCES TABLE

REAGENT or RESOURCE	SOURCE	IDENTIFIER
Antibodies		
mouse anti-Bruchpilot (1:100)	Developmental Studies Hybridoma Bank	Nc82, RRID:AB_2314866
rabbit anti-Discs large (1:1000)	(Frank et al., 2006; Hauswirth et al., 2018)	N/A
rabbit anti-GFP (1:1000)	Invitrogen	G10362, RRID:AB_221568
mouse anti-GFP (1:1000)	Invitrogen clone 3E6	A-11120
mouse anti-Repo (1:10)	Developmental Studies Hybridoma Bank	8D12, RRID:AB_528448
rabbit anti-H3 acetyl K9 (1:500)	abcam	ChIP grade ab10812, RRID:AB_297491
rabbit anti-H3 acetyl K14 (1:200)	abcam	ChIP grade ab52946, RRID:AB_880442
Alexa conjugated secondary antibodies (488, cy3, cy5) (1:300)	Jackson Immuno-research laboratories	N/A
Alexa Fluor 647 conjugated goat anti-HRP (1:100)	Jackson Immuno-research laboratories	N/A
Chemicals, Peptides, and Recombinant Proteins		
Philanthotoxin-433	Santa Cruz Biotechnology	276684-27-6
Critical Commercial Assays		
RNeasy Plus Micro kit	QIAGEN	74134
TURBO DNA-free	Ambion	AM1907
SuperScript III First-Strand synthesis system	Invitrogen	18080051
TaqMan® Fast Universal PCR Master Mix	Applied Biosystem	4352042
Experimental Models: Organisms/Strains		
dmp^{f07253}	Bloomington	BL19062 CG42543
dmp^{Mi}	Bloomington	BL60567
dmp RNAi	Bloomington	BL28299
ada2b^{EP}	Bloomington	BL31778 CG9638
ada2b RNAi	Bloomington	BL31347
ada2b^{1}	(Qi et al., 2004)	Jerry Workman (Stowers Institute, Kansas City, Missouri)
gcn5^{E333st}	Bloomington	BL9333 CG4107
gcn5^{Q186st}	Bloomington	BL9334
gcn5 RNAi	VDRC	v108943
sfg11^{e01308}	Bloomington	BL17941 CG13379
non-stop RNAi	Bloomington	BL28725 CG4166
GFP RNAi	Bloomington	BL9331
UAS-tdTomato	Bloomington	BL36328
UAS-Redstinger.nls	Bloomington	BL8546
UAS-GFP.nls	Bloomington	BL4776
Tubulin-Gal80^{ts}		Yuh-Nung Jan (University of California, San Francisco)
sar1 RNAi	VDRC	v108458 CG7073
UAS-ada2b-3HA	FlyORF	F000122
UAS-3hNC1	(Meyer and Moussian, 2009)	Bernard Moussian (Max-Planck-Institute for Developmental Biology, Tubingen, Germany)

(*Continued on next page*)

Continued

REAGENT or RESOURCE	SOURCE	IDENTIFIER
UAS-ES	(Meyer and Moussian, 2009)	Bernard Moussian (Max-Planck-Institute for Developmental Biology, Tubingen, Germany)
UAS-3hNC1-GFP	(Wang et al., 2014)	N/A
UAS-ES-GFP	(Wang et al., 2014)	N/A
NP6293-Gal4	(Stork et al., 2012)	Marc Freeman (Vollum Institute, Portland, Oregon)
Moody-Gal4	(Stork et al., 2012)	Marc Freeman (Vollum Institute, Portland, Oregon)
Alrm-Gal4	(Stork et al., 2012)	Marc Freeman (Vollum Institute, Portland, Oregon)
Repo-Gal4	(Keller et al., 2011)	N/A
Egr-Gal4	(Keller et al., 2011)	N/A
$Egr^{\Delta 25}$	(Keller et al., 2011)	N/A
Oligonucleotides		
Dmp_qPCR primer	Applied Biosystems	Dm01847117_g1
RpL32_qPCR primer	Applied Biosystems	Dm02151827_g1
Software and Algorithms		
GraphPad Prism (5.01)	GraphPad	N/A
MiniAnalysis (6.0.3)	Synaptosoft	N/A
Igor Pro (6.37)	WaveMetrics	N/A
Fiji	NIH	N/A
SlideBook	Intelligent Imaging Innovation	N/A

LEAD CONTACT AND MATERIALS AVAILABILITY

Further information and requests for resources and reagents should be directed to and will be fulfilled by the Lead Contact, Graeme Davis (Graeme.Davis@ucsf.edu).

All unique/stable reagents generated in this study are available from the Lead Contact without restriction.

EXPERIMENTAL MODEL AND SUBJECT DETAILS

Drosophila stocks were raised at room temperature on standard molasses food. *Drosophila* alleles used for RNAi knockdown experiments were raised at 25°C. For motoneuron-specific *Gal4* expression we used *OK371-Gal4* on the second chromosome. For muscle specific expression, we used *MHC-Gal4*. For glial specific expression, we used pan, perineurial, and subperineurial glial *Gal4* drivers as indicated in figure legends. Unless otherwise noted, the w^{1118} strain was used as a *wild-type* (*wt*) control. For temperature-dependent expression experiments, eggs were laid on apple plates and were maintained at 18°C. First-instar larvae with the right genotypes in the experimental group were selected and transferred to 29°C. Larvae in the control group were maintained at 18°C.

METHOD DETAILS

Electrophysiology

Sharp-electrode recordings were made from muscle 6 at abdominal segments 2 and 3 in third-instar larvae using an Axoclamp 2B or Axoclamp 900A amplifier (Molecular Devices). HL3 saline was used (in mM): 70 NaCl, 5 KCl, 10 $MgCl_2$, 10 $NaHCO_3$, 115 Sucrose, 5 Trehalose, 5 HEPES, and 0.3 $CaCl_2$ (unless specified otherwise). EPSP and mEPSP traces were analyzed in Igor Pro (WaveMetrics) with previously published routines and MiniAnalysis (Synaptosoft) (Gaviño et al., 2015). For the rapid induction of synaptic homeostasis, larvae were incubated in 15μM Philanthotoxin-433 in an un-stretched, partially dissected preparation (PhTX, Santa Cruz Biotechnology) for 10min (Frank et al., 2006). For each NMJ, the average amplitudes of evoked EPSP are based on the mean peak amplitudes in response to 20-30 individual stimuli. Spontaneous mEPSPs were recorded continuously 60-90 s. Quantal content was estimated for each NMJ as the ratio of EPSP amplitude/mEPSP amplitude. The mean value across all NMJ for a given genotype is reported. All statistics analyses were performed in GraphPad Prism.

Immunocytochemistry

Standard immunocytochemistry was performed as previously described (Wang et al., 2014). Briefly for total immunostaining: dissected third instar larvae were fixed with 4% PFA in PBS for 20min and incubated with primary antibody diluted in PBST (PBS with 0.5% Triton-100) overnight at 4°C after six brief washes with PBST. Larvae were then incubated with secondary antibody diluted in PBST for 1.5hr at room temperature and mounted in Vectorshield without DAPI (otherwise specified in Figure Legends or Results, Vector Laboratories) after six brief washes with PBST. For surface Multiplexin immunolabeling, dissected third instar larvae were incubated with primary antibody for 20min at room temperature and fixed with ice-cold ethanol. For surface GFP immunolabeling, dissected third instar larvae were incubated with mouse anti-GFP antibody for 20min at room temperature and fixed with 4% PFA in PBS.

Image Acquisition

Confocal imaging for peripheral nerves and synapses was performed on a Yokagawa CSU22 spinning disk confocal with a 60x/1.4 plan Apochromat objective. Z stacks of peripheral nerves or NMJ on muscle 6/7 were acquired and maximum projections were used for analysis. Confocol images for the ventral nerve cords were acquired using an Andor Zyla sCMOS camera mounted to a Nikon Ti Microscope with an Andor Borealis CSU-W1 spinning disc confocal with a Nikon Plan Apo 20x/0.75. Deconvolution imaging for synapse morphology was performed using a Plan Apo objective 60x/1.4 (Carl Zeiss) on an Axiovert 200 inverted microscope (Carl Zeiss) equipped with a cooled CCD camera (CoolSNAP HQ; Roper Scientific). Image acquisitions were performed in SlideBook software (Intelligent Imaging Innovation).

Quantitative RT-PCR

Quantitative RT-PCR was performed as previously described (Bergquist et al., 2010; Müller et al., 2012; Younger et al., 2013), with slightly modified procedures. Primer probes specific for real-time PCR detection of Multiplexin (Dmp, Dm01847117_g1) and Ribosomal protein L32 (RpL32, Dm02151827_g1) were designed and developed by Applied Biosystems. The brains were removed from 5 third-instar larvae (3 replicates/genotype) and RNA isolation was performed immediately (RNeasy Plus Micro kit, QIAGEN). Potential DNA contamination was removed (TURBO DNA-free, Ambion) and single-strand cDNA libraries were prepared with SuperScript III First-Strand synthesis system (Invitrogen).

QUANTIFICATION AND STATISTICAL ANALYSIS

Statistics

Quantification of data are presented as mean ± standard error of the mean (SEM) with the precise N numbers indicated in the figure legends or the supplemental table. Statistical analysis was performed using Prism (5.01, GraphPad) and using paired two-tailed Student's t test or one-way ANOVA as indicated in the figure legends.

Quantitative Image Analysis

Maximum projections of deconvolved or confocal images were used for analyses. Quantification of Brp and bouton number (Figure 3) was performed as previously described (Frank et al., 2009) with Watershed Segmentation plugin in Fiji software (NIH). For H3K9Ac and H3K14Ac average fluorescence intensity analyses (Figure 4), individual Egr positive nuclei on proximal peripheral nerves were traced and analyzed for each genotype in Fiji (NIH). Mean of the average fluorescence intensity of each nucleus quantified were reported. For Multiplexin-GFP average fluorescence intensity analysis (Figure 7), GFP signal is amplified by mouse anti-GFP antibody and the average fluorescence intensity is measured in ROIs generated by tracing the GFP expressing cells/segments at the NMJ (muscle 6/7) and along peripheral nerves that innervate muscle 6/7. GFP intensity in ventral nerve cord is quantified as the average fluorescence intensity of the VNC (optical lobes not included). All analyses were performed using Fiji software (NIH) and statistics analyses were performed in GraphPad Prism.

DATA AND CODE AVAILABILITY

This study did not generate datasets for public repositories or new data code.